Mon. Not. R. Astron. Soc. **000**, 000–000 (0000) Printed 2 February 2008 (MN LATEX style file v2.2)

A 2dF survey of the Small Magellanic Cloud

Christopher J. Evans[1⋆], Ian D. Howarth[2],
Michael J. Irwin[3], Adam W. Burnley[2] & Timothy J. Harries[4]
[1] *Isaac Newton Group of Telescopes, Apartado de Correos 321, 38700 Santa Cruz de la Palma, Canary Islands, Spain*
[2] *Department of Physics and Astronomy, University College London, Gower Street, London WC1E 6BT, UK*
[3] *Institute of Astronomy, University of Cambridge, Madingley Road, Cambridge CB3 0HA, UK*
4*School of Physics, University of Exeter, Stocker Road, Exeter EX4 4QL, UK*

Received:

ABSTRACT
We present a catalogue of new spectral types for hot, luminous stars in the Small Magellanic Cloud. The catalogue contains 4161 objects, giving an order of magnitude increase in the number of SMC stars with published spectroscopic classifications. The targets are primarily B- and A-type stars (2862 and 853 objects respectively), with 1 Wolf-Rayet, 139 O-type, and 306 FG stars, sampling the main sequence to ∼mid-B. The selection and classification criteria are described, and objects of particular interest are discussed, including UV-selected targets from the Ultraviolet Imaging Telescope (UIT) experiment, Be and B[e] stars, 'anomalous A supergiants', and composite-spectrum systems. We examine the incidence of Balmer-line emission, and the relationship between Hγ equivalent width and absolute magnitude for BA stars.

Key words: galaxies: Magellanic Clouds – stars: early-type – stars: emission-line, Be – stars: fundamental parameters – stars: Hertzsprung-Russell diagram

1 INTRODUCTION

Since the seminal study of the solar-neighbourhood stellar initial mass function (IMF) by Salpeter (1955), there have been numerous observational and theoretical studies of the IMF in the Galaxy, the Magellanic Clouds, and beyond (cf. Gilmore & Howell 1998). One of the principal tools used in the investigation of the IMF is the comparison of observed Hertzsprung-Russell diagrams (HRDs) with those obtained from population syntheses built on stellar-evolution models. The construction of observational HRDs for large samples of roughly equidistant stars is most easily accomplished in the colour–magnitude plane. However, optical observations only sample the Rayleigh-Jeans tail of the spectral energy distribution of O- and early B-type stars; thus for these objects optical photometric colours alone do not provide adequate discrimination in temperature (nor, therefore, in luminosity) for satisfactory transformation between the observed and theoretical HRDs.

The Small Magellanic Cloud (SMC) is of particular interest as the nearest system with a well-established, substantial (factor ∼5) underabundance of metallic elements compared to those found in the Milky Way. This makes it an attractive target for investigating the role of metallicity in star formation and evolution, as well as a variety of other topics in stellar and galactic astrophysics. With this in mind, we have undertaken a spectroscopic survey of the SMC's hot, luminous stars, using the multi-fibre 2-degree Field (2dF) instrument of the Anglo-Australian Telescope (AAT), primarily in order to investigate directly the massive-star IMF.

The basic data of the 2dF spectroscopic survey are presented in this paper, wherein catalogue entries are identified by '2dFS' numbers for convenience. Target selection, observations and data reduction are described in Section 2, while the criteria used for spectral and luminosity classification of the sample are discussed in Sections 3 and 4. Some aspects of the photometry are discussed in Sections 5 and 6. Observations of stars of particular interest are presented in Section 7, and catalogue contents are summarized in Appendix A. An investigation of the IMF of the SMC, based in part on the catalogue, will be presented elsewhere.

2 DATA ACQUISITION

2.1 Target selection: input catalogue

Our initial aim was to use photometry to isolate those targets for which spectroscopy was required for accurate placement in the HRD. The actual targets were then to be drawn from this input catalogue.

At the start of the project, the best available source for both large-scale photometry and accurate astrometry (es-

⋆ email: cje@ing.iac.es; idh@star.ucl.ac.uk; mike@ast.cam.ac.uk; awxb@star.ucl.ac.uk; th@astro.ex.ac.uk

Table 1. 2dF field centres. The fields were observed in 1998 (September 25–28, fields 1–12) and 1999 (September 30/October 1, fields 13–18).

Field no.	Field centre (J2000) α	δ	Integration time (min)
1	01 21 16.7	−73 14 19	60
2	01 21 16.7	−73 14 19	120
3	00 41 53.2	−73 33 33	150
4	00 41 53.2	−73 33 33	150
5	01 06 32.4	−72 43 58	90
6	01 06 31.1	−73 03 58	120
7	00 48 47.9	−73 03 39	120
8	01 06 31.1	−73 03 58	150
9	01 26 12.1	−73 14 27	120
10	01 06 30.5	−73 13 58	120
11	01 11 25.8	−73 14 05	120
12	00 59 37.3	−73 08 50	90
13	01 00 00.0	−72 40 00	60
14	00 59 00.0	−72 55 00	90
15	01 00 00.0	−72 45 00	90
16	00 44 00.0	−73 24 00	94
17	00 58 00.0	−72 40 00	90
18	01 10 00.0	−72 55 00	86

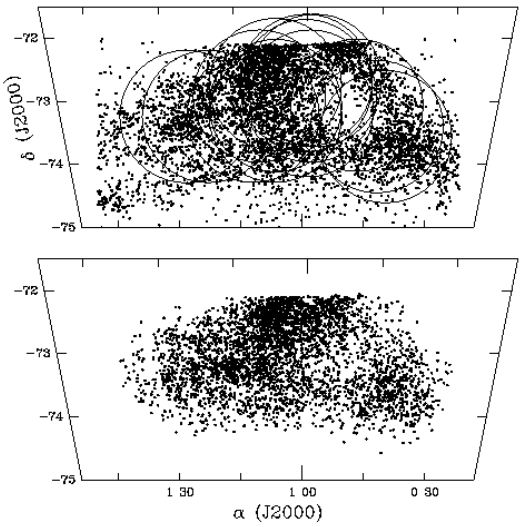

Figure 1. Spatial distribution of the input catalogue (every 5th star, upper panel, observed fields shown as 2° circles) and the spectroscopically observed targets (all targets, lower panel).

sential for the 2dF observations) was scans of UK Schmidt B_J[1] and R photographic survey plates made with the Automatic Plate Measuring (APM) machine. Field #29 in the Schmidt survey covers the greater part of the SMC and was used to compile the input catalogue of potential targets. The densest regions (e.g., NGCs 330 and 346) were too crowded for reliable APM scans and are largely excluded from our work.

For our investigation of the upper part of the IMF (and to avoid contamination by foreground stars) the APM targets making up the input catalogue for spectroscopy were restricted to bright blue stars, with cuts of $(B_J - R) < 0.1$ (corresponding, notionally, to O and B spectral types) and $B_J < 17.5$. As the survey and analysis progressed, it became evident both that additional selection effects were in play (most importantly, systematic rejection of the brightest stars as 'non-stellar'), and that the photographic photometry had rather larger uncertainties than anticipated. These additional sampling effects will be discussed in our forthcoming analysis of the IMF (and a more detailed discussion of photometry is given in Section 5), but one consequence is that the colour cut-offs were not as effective as expected in isolating only the hottest stars. As a result, some relatively red stars were included in the observed 2dF sample, including foreground objects. (The expected surface density of foreground blue stars is negligibly small – about 1 per square degree.) Fortunately, although our 2dF observations were not generally optimized for radial-velocity measurements, they are quite sufficient to discriminate between typical Galactic and SMC velocities ($\sim$+170 km s^{-1}). Radial-velocity measurements identified 171 stars, mostly in the spectral range G0–K3, as probable foreground objects. These targets were discarded for the purposes of the spectroscopic catalogue.

[1] B_J indicates the use of Eastman Kodak IIIa-J emulsion (+GG495 filter); $B_J \simeq B - 0.28(B - V)$ (Blair & Gilmore 1982).

2.2 2dF observations

The 2dF system is a dual-spectrograph, multi-fibre instrument which allows up to 400 intermediate-dispersion spectra to be obtained simultaneously across a two-degree diameter field of view (Lewis et al. 2002). We used 2dF to observe 18 overlapping SMC fields over 1998 September 25–28 and on 1999 September 30 & October 1 (Table 1). The Moon was below the horizon for the majority of the observations, the exceptions being fields 1, 4, 5, 9, and 10 (Moon before first quarter) and 18 (barely gibbous moon just risen, $\sim$100° from the SMC). In a typical observation approximately 30 'sky' fibres ($\sim$15 for each spectrograph) were assigned, to ensure good definition of the sky signal.

In order to construct a spectroscopic catalogue that is statistically representative of the SMC population of hot, luminous stars, targets were selected from the input catalogue essentially at random.[2] The main selection criterion was, therefore, simply the set of physical constraints imposed in configuring 2dF (e.g., avoidance of too-close fibre heads, large angular deflections of fibres, etc.), rather than any astrophysical characteristics of the stars beyond those chosen in constructing the input catalogue. Usable spectra were obtained for $\sim$15% of the input catalogue, with a reasonably representative spatial sampling (Figure 1).

We used gratings ruled at 1200 lines/mm, which gave coverage of the $\sim$3900–4800Å region (Hβ is included in about half the spectra) at a resolution of $\sim$2.75Å (FWHM of arc lines; $R \simeq 1500$), which corresponds to 2.5 pixels on the detectors. Individual exposures were normally 1800s, and the median continuum signal-to-noise in the region $\lambda\lambda$4395–4460 is $\sim$45, ranging $\sim$20–150.

Two 2dF datasets were obtained in addition to this main spectroscopic sample. First, usable red (Hα) spectra were

[2] In 1999, some effort was made to redress systematic underrepresentation of bright stars in the 1998 run.

obtained for 1091 targets from the main sample during the 1999 run (September 28 & 29), again using gratings with 1200 lines/mm ($R \simeq 2500$).

Secondly, in 2001 September, when conducting the programme of observations of SMC binaries described by Harries, Hilditch & Howarth (2003), we were able to allocate 'spare' fibres to targets of interest, with essentially the same instrumental setup as in 1999. We chose to observe UV-selected targets from the UIT catalogue (Cornett et al. 1997; Parker et al. 1998) because of their potential interest as an important component of the hot-star population of the SMC. Because of the different selection criteria applied, the 107 targets so observed are separately numbered in the catalogue: 2dFS#5001–5107.

2.3 2dF data reduction

The bulk of the data reduction was performed using the 2dfdr software (Lewis et al. 2002). The main steps include bias subtraction, extraction of the spectra from the CCD image, optional division by a normalized flat-field, wavelength calibration, calibration of the fibre throughputs, and subtraction of the scaled median sky spectrum. The software was still undergoing active development at the time of our reductions, and had been most extensively tested on datasets quite different to ours (namely, the 2dF quasar and galaxy survey data), so that a number of manual checks and interventions were necessary.

2.3.1 Flat-fielding

At the time of the reductions flat-fielding in 2dfdr was suboptimal, because any flexure in the spectrographs led to the extraction of different flat-field pixels compared to those used in the object frame. Given the reasonable cosmetic quality of the detectors (and our familiarity with 'known' instrumental features) we elected not to flat-field our spectra.

2.3.2 Throughput calibration

Depending on the configuration, the throughput of individual fibres is known to vary at the ∼10% level (separately to the issue of targets being well centred on the fibre), probably because of differing stresses within the fibres. Accurate throughputs are necessary for reliable subtraction of the sky signal (which is scaled from sky-only fibres by the relative fibre transmission factors).

At the time of our observations, the normal method of obtaining the relative throughputs was to take offset-sky exposures in dithered triplets (to minimize contamination from astrophysical sources) for each fibre setup. Observatory recommendations for offset-sky integrations in 1998 (300s) yielded rather low signal-to-noise for our setup, so longer exposures were used in 1999 (450s), notwithstanding the larger overheads, together with twilight throughput frames. Twilight frames were acquired in 1998 for only two fields (of course, only the first and last configurations each night can use these flats for throughputs), the conventional wisdom at that time (when 2dF observing procedures were still under development) being that the sky brightness varied significantly across the 2° field of 2dF.

We found the twilight frames to be entirely consistent with the offset (dark) skies, with much better signal to noise ratio. This conclusion is retrospectively supported by the observations of Chromey & Hasselbacher (1996), who measured the relative brightness gradient of the twilight sky as a function of angle from the horizon point nearest the Sun. The 2dF twilight frames were taken with a maximum zenith distance of 30°, i.e. the angle between the solar horizon and the observed region of twilight sky is between 60 and 120°. In this range Chromey & Hasselbacher found that the largest observed relative gradient is ±2% per degree of sky, which is negligible for our sky-correction purposes.

2.3.3 Final spectra

In a number of cases we have repeat observations of a given target (usually to build up signal-to-noise). The 2dfdr algorithm for combining spectra from separate exposures resulted in nonsensical results in some cases (e.g., negative fluxes from the sum of positive fluxes). 2dfdr has since undergone development to remove some of these problems, but we simply summed the net signals, while looking for (and rejecting) discrepant points; this proved particularly effective at removing cosmic-ray signatures.

Once combined, the spectra were roughly rectified using a script that fits a polynomial to predefined continuum regions and then divides the spectrum through by the fit. This automated rectification gives significant time savings and still allows accurate spectral classification. Final manual rectifications were conducted as necessary.

2.4 Long-slit observations

A limited number of supplementary observations of 2dF targets were obtained in conventional long-slit mode, using the Royal Greenwich Observatory (RGO) Spectrograph at the AAT in July 2001. Ruled 1200/mm gratings were used to obtain blue (∼3700–5500Å) and red (∼5250–7050Å) spectra. The mean resolution element, as defined by the comparison arcs, was 1.6Å FWHM, equivalent to 3.7 pixels. Standard 'optimal' extractions were performed on these spectra, which generally have continuum S/N ratios of ∼100 or better.

The purpose of these observations was not only to obtain repeat spectra of selected stars of interest, but also to provide a check on the 2dF data characteristics. This was considered important in view of the limited experience of observing 'bright', absorption-line objects with 2dF at the time of our observations, and because the spectra were extracted with development versions of 2dfdr. As discussed in Section 6.2.2, the long-slit observations disclose no obvious problems with the fibre spectra.

3 SPECTRAL CLASSIFICATION

The 2dF spectra (which consist primarily of B- and A-type stars, with a minority of O-, F-, and G-types) were classified primarily by visual inspection, guided by the temperature-sequence classification criteria summarized in Table 2.

Table 2. Primary temperature-sequence classification criteria applied to the 2dF sample (see Section 3 for references). Only some O subtypes are given here, others being interpolated.

Type	Criteria
O6	He II λ4200 $\sim$ He I + II λ4026
O7	He II λ4541 $\sim$ He I λ4471
O8.5	He II λ4541 $\sim$ He I λ4387
O9	He II λ4200 $\sim$ He I λ4143
B0	He II $\lambda\lambda$4686, 4541 present, λ4200 weak
B0.5	He II $\lambda\lambda$4200, 4541 absent, λ4686 weak
B1	He II λ4686 absent, Si IV $\lambda\lambda$4088, 4116 present
B1.5	Si IV λ4116 absent, Si IV λ4088 $<$ O II
B2	Si IV, Si II absent, Si III λ4553 $>$ Mg II λ4481
B2.5	Si III λ4553 $\sim$ Mg II λ4481
B3	Si III λ4553 $<$ Mg II λ4481
B5	Si III absent, Si II λ4128/4132 $<$ He I λ4121
B8	He I λ4121 $<$ Si II $<$ He I λ4143
	Mg II λ4481 $\leq$ He I λ4471
B9	Mg II λ4481 $>$ He I λ4471
	Fe II λ4233 $<$ Si II λ4128/4132
A0	Ca K/(Hϵ + Ca H) $<$ 0.33
A2	0.33 $<$ Ca K/(Hϵ + Ca H) $<$ 0.53
A3	0.53 $<$ Ca K/(Hϵ + Ca H) $<$ 0.75
A5	0.75 $<$ Ca K/(Hϵ + Ca H) $<$ 0.85
A7	0.85 $<$ Ca K/(Hϵ + Ca H) $<$ 0.95
F0	Ca K/(Hϵ + Ca H) $\sim$1
F5	Clear presence of CH G-band
F8	G-band/Hγ = 0.5–0.75
G0	G-band/Hγ = 0.75–0.9
G2	G-band $\sim$ Hγ; Hγ $>$ Fe I λ4325
G5	Hγ $\sim$ Fe I λ4325
G8	Hγ $<$ Fe I λ4325

3.1 O-type spectra

Digital spectra are widely available for O-type stars, and the principal reference we used for the O stars observed with the 2dF was Walborn & Fitzpatrick (1990). The primary classification criteria are the ratios of He I to He II, so the spectral types are largely unaffected by metallicity effects. Luminosity classes were assigned using the precepts given by Walborn & Fitzpatrick (1990), with reference to the SMC spectra shown in Walborn et al. (2000). Examples of 2dF O-dwarf spectra are shown in Figure 2.

3.2 B-type spectra

3.2.1 Temperature sequence

For the B-type stars the principal reference we adopted was Lennon's (1997) study of SMC B-type supergiants; the primary classification criteria used here are included in Table 2, and, excepting the very earliest subtypes, use metal lines.

The overall strength of the metallic lines in B-type spectra is related to the luminosity: the more luminous the star, the stronger the lines (e.g., Walborn & Fitzpatrick 1990). The majority of the 2dF targets are substantially less luminous than those in Lennon's sample; thus the metal lines in the 2dF B-star spectra are weak both because of the reduced metallicity of the SMC, and also because of their relatively low luminosity. As a consequence, while some of the 2dF spectra can be precisely classified following Lennon's scheme, the large majority require coarser classification bins, even where the data quality is moderately good.

By way of illustration, consider a mid-B giant where the Si III λ4553 line is undetectable. This may be because it is B5 or later, or because it is slightly hotter (e.g., B3) but, due to luminosity effects, the Si III line is weak and in the noise. These problems mainly arise in the B1–B5 range, where the primary criteria involve the ratios of Mg II λ4481 and Si III. Inspection of Lennon's data also reveals that the O II λ4415–17, 4640-50 and N II λ4631 features are undetectable at B3 and later; when observed, these features therefore allow the spectral type to be more closely bracketed, to B1–B3.

In Lennon's scheme, type B1 is characterized by weak or absent He II λ4686; however, the 2dF spectra are at lower resolution than his data ($\sim$2.5–3 vs 1.2Å), and poorer signal-to-noise. The framework adopted here uses the intermediate B0.5 type for those stars where He II $\lambda\lambda$4200, 4541 are absent and weak λ4686 is seen.

Examples of precisely classified 2dF B-type spectra are shown in Figure 3; further examples, where precise classification was not possible (even at fairly good S/N), are shown in Figure 4. The spectrum of 2dFS#2195 is included in Figure 4 as an example of the low signal-to-noise 2dF data; the star is clearly of early-B type (given the absence of strong He II lines and the strength of the He I lines), but cannot be more accurately classified. A similar classification is applied to the spectrum of 2dFS#1492, even though the data are of substantially better quality. It is not possible to be confident that the weak He II lines seen in, e.g., 2dFS#0482 are absent in #1492, and the metal lines necessary for unique classification in the early B-stars are not seen (as in 2dFS#1931).

Many of the B-type spectra display emission in one or more of the Balmer lines (see Section 7.1). Where double-peaked or resolved Balmer emission is evident, an 'e' qualifier is adopted (see Section 7.2).

3.2.2 Luminosity classification

In principle, luminosity-class assignments can be made using combinations of features, as for Galactic stars, modified to account for the systematic differences in metal-line strengths (e.g., Walborn 1977). We attempted to classify the B-type stars in our sample using this approach, but were handicapped by the generally inadequate signal-to-noise of our data. We were therefore forced to fall back on the use of the Balmer lines alone, and particularly Hγ. Notwithstanding potential pitfalls (cf. Jaschek & Jaschek 1990), this provides the simplest criterion for luminosity classification of B (and A) stars.

We measured the Hγ equivalent widths, W$_\lambda$, in the entire 2dF sample 'by hand', and by using an automated gaussian-fitting procedure. In addition to W$_\lambda$, the gaussian fits yield the actual line width, characterized by full width at half depth. Excepting a small minority of pathological cases (e.g., stars with strong line-core emission, where the automated fits give erratic results), all three measures lead to essentially identical conclusions in respect of classifications; in particular, the automated and 'by hand' equivalent widths are in excellent agreement. For reasons of objectivity and reproducibility, we generally utilize the gaussian-fit equivalent widths.

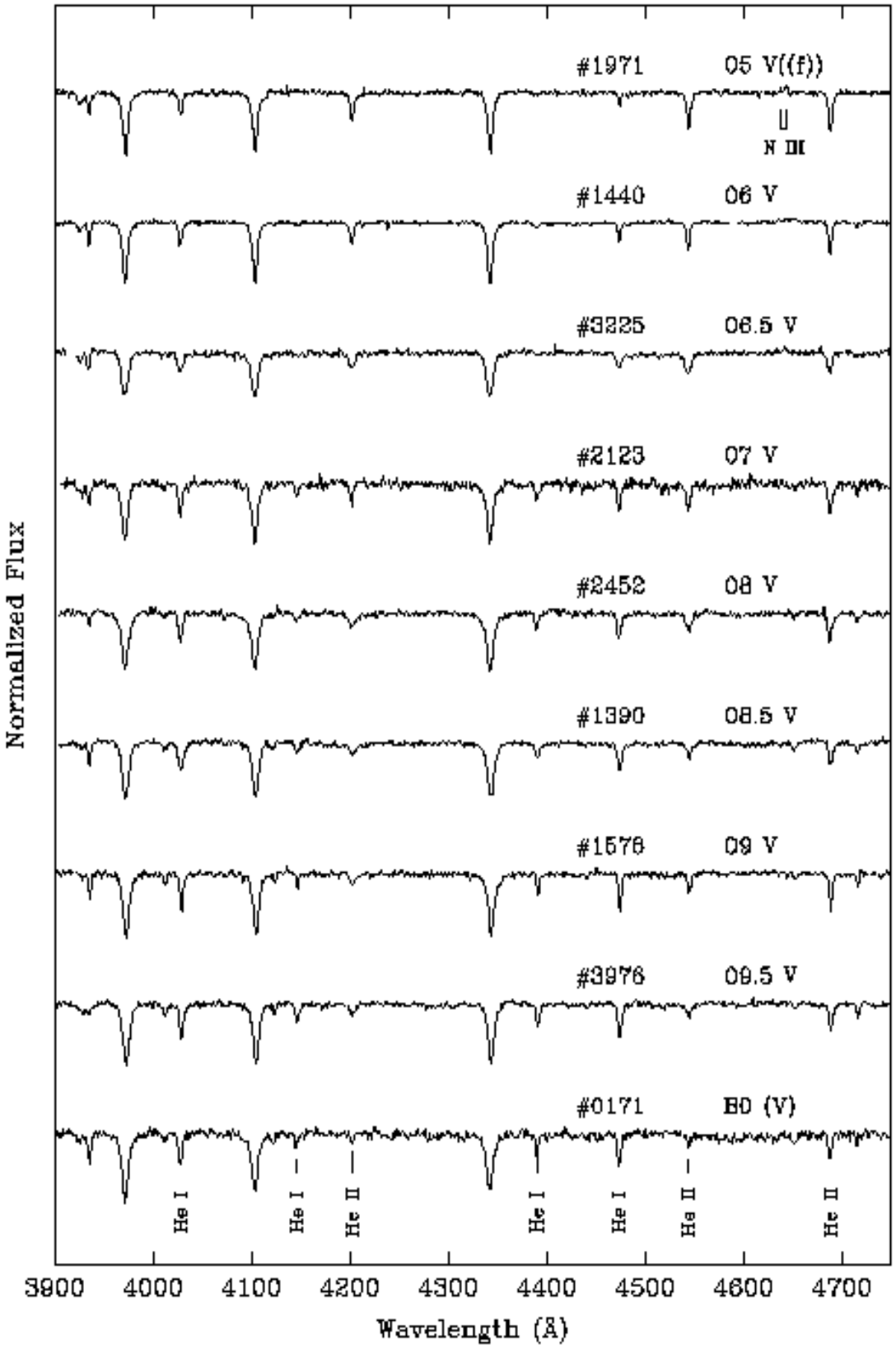

Figure 2. 2dF SMC spectra – I: O-dwarf spectral sequence. Stars are identified by 2dFS catalogue number. The luminosity class for the B0 star is assigned using the hybrid scheme described in Section 3.2.2. The spectral lines identified in 2dFS#0171 are, from left to right by species, He I $\lambda\lambda$4026, 4143, 4388, 4471; He II $\lambda\lambda$4200, 4541, 4686. The Balmer lines Hϵ λ3970, Hδ λ4101 and Hγ λ4340 are not explicitly identified. Note the weak N III λ4634-40-42 emission and strong He II λ4686 absorption in 2dFS#1971, giving rise to the '((f))' suffix. Successive spectra are vertically offset by 0.75 continuum units.

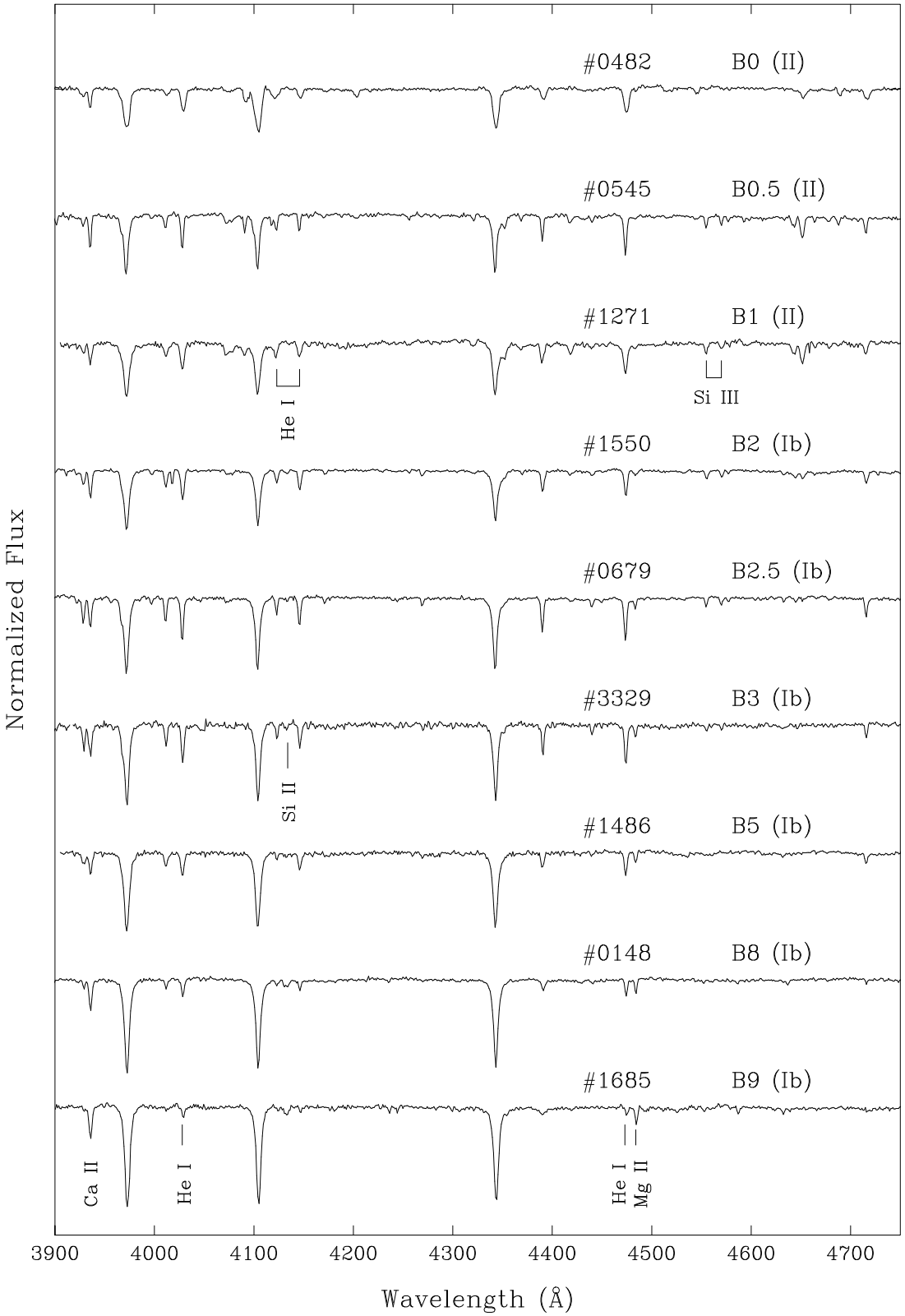

Figure 3. 2dF SMC spectra – II: B spectral sequence. Stars are identified by 2dFS catalogue number. The parenthesised luminosity classes indicate their origin in the hybrid scheme described in Section 3.2.2. The spectral lines identified in 2dFS#1685 are, from left to right, Ca II λ3933 (Ca K), He I $\lambda\lambda$4026, 4471 and Mg II λ4481. The silicon feature identified in #3329 is Si II λ4128/4132 and the additional lines in #1271 are He I $\lambda\lambda$4121, 4143 and Si III $\lambda\lambda$4553, 4568. Successive spectra are vertically offset by 0.75 continuum units.

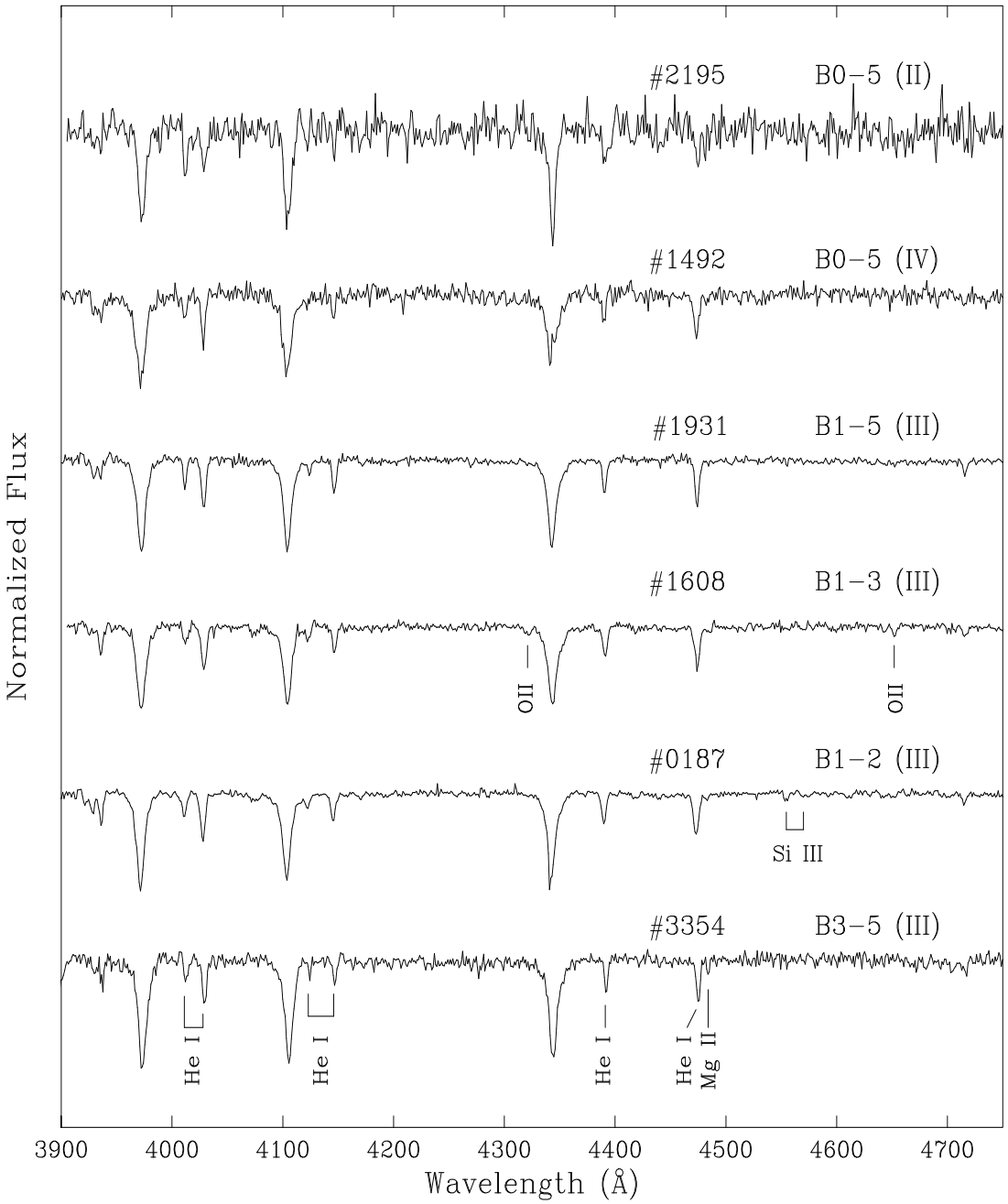

Figure 4. 2dF SMC spectra – III: Exampes of B-type spectra without precise classifications; cf. Section 3.2.1 for details. Stars are identified by 2dFS catalogue number. The parenthesised luminosity classes indicate their origin in the hybrid scheme described in Section 3.2.2. The wavelengths of the identified lines are given in Figs. 2 and 3 with the addition of He I λ4009 in 2dFS#3354 and the O II λ4317–19 and 4650 blends in #1608. Successive spectra are vertically offset by 0.75 continuum units.

Ideally, our luminosity-class assignments should be based exclusively on spectral morphology. Unfortunately, the spread in Hγ equivalent width is fairly large at given B magnitude (as discussed further in Section 6); equivalently, the range in $M(B)$ at given W$_\lambda$ is considerable. Thus our W$_\lambda$ data, which are not particularly accurate because of the limited signal-to-noise ratio in the spectra, are of rather limited utility in predicting absolute magnitude and, by inference, luminosity class, particularly at early-B types, where stars with the same W$_\lambda$ are found at all luminosity classes (cf. Fig 10; B0 V and B0 I stars differ in W$_\lambda$ by only $\sim$2Å, comparable with the spread in the measurements). Faced with this difficulty, and after considerable experimentation, we reluctantly abandoned the principled position of luminosity classification based solely on morphology in favour of a

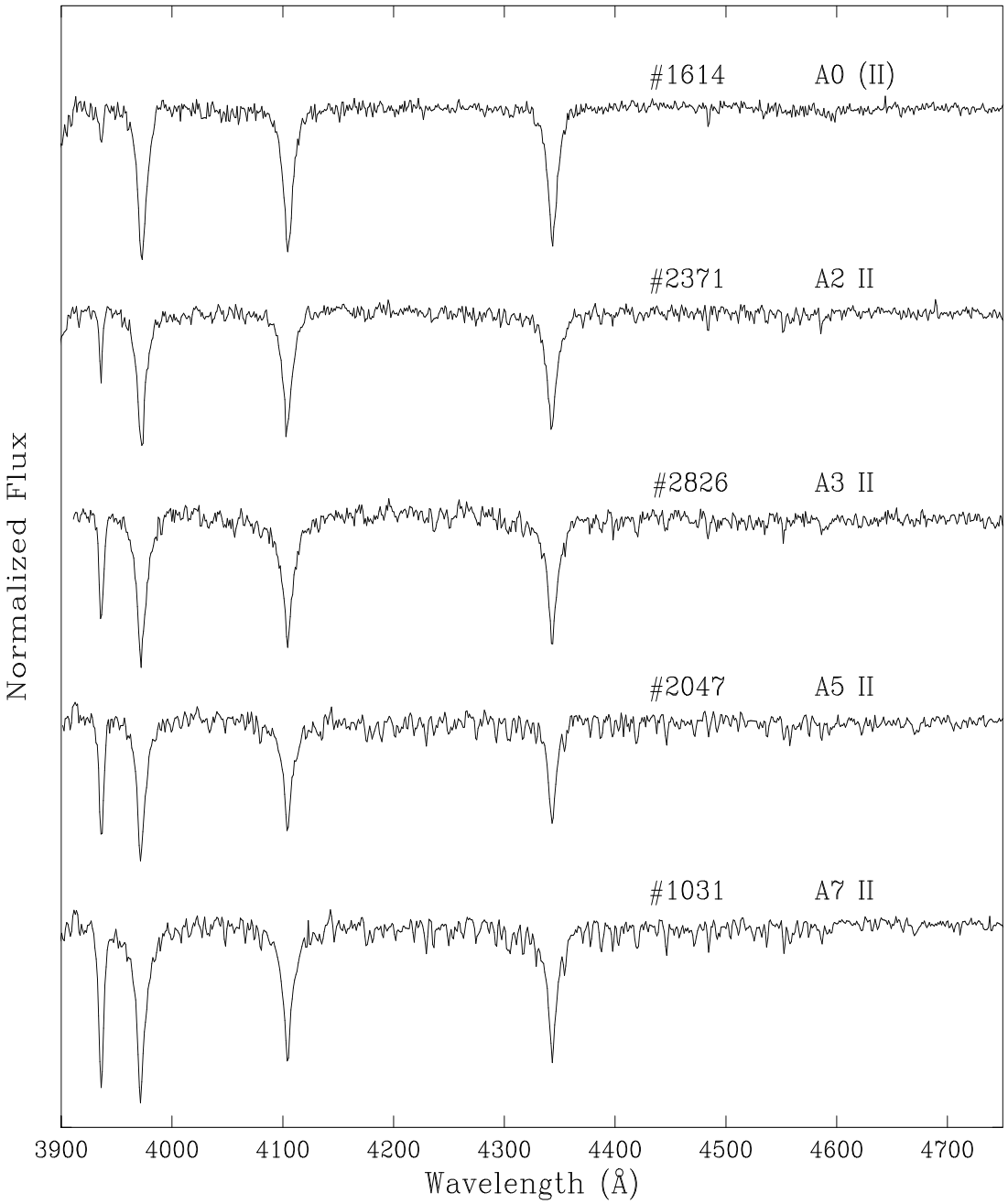

Figure 5. 2dF SMC spectra – IV: Exampes of A-type spectra. Stars are identified by 2dFS catalogue number. The luminosity class for the A0 star is assigned using the hybrid scheme described in Section 3.2.2. Successive spectra are vertically offset by one continuum unit.

more pragmatic approach incorporating absolute-magnitude information.

The (ad hoc) formulation we adopted is that the boundaries between luminosity classes are defined by loci of constant $B + 0.3\mathrm{W}_\lambda$, as listed in Table 3. To define the boundaries, we adopted the relationship between $M(V)$ and luminosity class given by Humphreys & McElroy (1984), augmented by Schmidt-Kaler (1982) as necessary, and converted to B by adopting $(B-V)_0$ colours from Fitzgerald (1970) and an *apparent* distance modulus of 19.2, from Harries et al. (2003). The equivalent width corresponding to each B magnitude was then determined directly from the data (cf. Section 6).

Clearly, the resulting 'luminosity classes' are not true, MK-process, morphological types, and to make this clear the luminosity-class assignments derived through the hybrid photometric/spectroscopic approach are given in parentheses in the catalogue, and throughout this paper. Nonetheless, the hybrid classifications do appear to be broadly consistent with results from other sources (Section 4.1), although for

Table 3. B-star luminosity-class criteria: boundary values of the parameter $B + 0.3W_\lambda$ (cf. Section 3.2.2). Parentheses are used to indicate that these are not true morphological luminosity classes, but are based on both spectroscopic *and* photometric criteria.

Sp. Type	Luminosity Class (Ia)	(Iab)	(Ib)	(II)	(III)	(IV)	(V)
B0	12.27	12.92	13.35	13.96	14.80	15.57	
B0.5	12.30	12.95	13.82	14.43	14.82	15.60	
B1	12.34	13.12	14.00	14.92	15.76	16.47	
B1.5	12.09	13.14	14.09	15.27	16.35	17.07	
B2	12.10	13.15	14.23	15.54	16.63	17.41	
B2.5	12.16	13.20	14.28	15.73	16.81	17.72	
B3	12.48	13.39	14.40	16.18	17.72	18.63	
B5	12.71	13.49	14.69	16.99	18.86	19.51	
B8	13.11	13.88	15.26	18.19	20.54	21.18	
B9	13.22	14.37	15.96	18.91	21.37	21.90	
A0	13.37	14.60	16.86	20.10	22.16	22.76	

spectra where Hγ is filled in by emission our assigned luminosity classes are liable to be too bright. For stars of particular interest, investigators should therefore refer to the notes on Balmer emission that we provide for every star (Section 7.1; Appendix A).

3.3 A-type stars

3.3.1 Temperature sequence

The A-type stars were classified on the basis of the Ca K/Hϵ line ratio, as discussed by Evans & Howarth (2003). Reliance on the calcium line ratios is not without its problems (see discussion in Evans & Howarth), but it is quick to apply and does not rely on weak metal lines. The classification criteria from Evans & Howarth are included in Table 2. Figure 5 illustrates a spectral sequence, and Section 7.4 discusses a handful of peculiar A stars.

3.3.2 Luminosity classification

Evans & Howarth (2003) describe observations of a number of Galactic BAF stars acquired for comparison and calibration purposes. We have supplemented those observations with some new data, giving a total of 46 A-type stars (Table 4). We measured Hγ in these Galactic standards in the same way as in our 2dF sample, in order to calibrate line strength and luminosity class as a function of spectral subtype. All the available data are consistent with the simple luminosity-class–equivalent-width scheme summarized in Table 5, which is independent of A spectral subtype for the observed Galactic standards.

The adopted luminosity-class bins are broadly consistent with the calibrations given by Balona & Crampton (1974) and Azzopardi (1987), except that Azzopardi's equivalent widths are 1–2Å (∼30–50%) larger than ours for late-A supergiants. This discrepancy appears to arise because Azzopardi's (mainly interpolated) late-A values are influenced by Hγ equivalent widths for F-type stars that are larger than we find (Section 6.1). Although late-A, bright supergiants are not well represented in either sample, our dataset is more extensive, and of better quality, than his.

Table 4. Galactic A-type stars observed for calibration purposes. Most of these are discussed by Evans & Howarth (2003); new stars are identified by lower-case spectral-type sources.

HD	Spectral type	Source	HD	Spectral type	Source
1404	A2 V	GG7	175687	A0 II	c69
1457	A9 Ib–II	g01	186177	A5 II	g01
3283	A3 II	GG9	187983	A1 Iab	M55
3940	A1 Ia	M55	192514	A3 III	S54
8538	A5 V	M53	195324	A1 Ib	C69
10845	A8 III	GG9	196379	A9 II	M73
12216	A1 V	S54	197345	A2 Ia	M73
12279	A0 V	GG7	197489	A5 II	g01
12953	A1 Ia	M55	201935	A5 II	g01
13041	A4 V	GG9	202240	A8 II	g01
13476	A3 Iab	M55	203280	A7 IV–V	M53
14433	A1 Ia	m55	205835	A5 V	GG9
14489	A2 Ia	M55	207260	A2 Ia	M55
14535	A2 Ia p:	m55	207673	A2 Ib	M55
15316	A3 Iab	M55	210221	A3 Ib	M55
17378	A5 Ia	M55	211868	A5 Ib–II	g01
148743	A7 Ib	G01	212511	A3 II	g01
161695	A0 Ib	C69	213558	A2 V	S54
164514	A5 Ia	m55	213973	A9 III	A81
165784	A2 Ia	m55	216701	A7 IV	GG9
167356	A0 Ia	m55	220770	A5 Ib	m55
172167	A0 V	M73	222275	A5 III	A85
173880	A3 V	GG9	223385	A3 Ia	M55

Sources of spectral types are (in order of preference): M73, Morgan & Keenan (1973); M43, Morgan et al. (1943); M55, Morgan et al. (1955); M53, Morgan et al. (1953); M50, Morgan & Roman (1950); S54, Slettebak (1954); GG7, Gray & Garrison (1987); GG9, Gray & Garrison (1989); A81, Abt (1981); A85, Abt (1985); G01, Gray et al. (2001); C69, Cowley et al. (1969).

Table 5. Adopted luminosity-class criteria: luminosity class for A2–A7 stars as a function of Hγ equivalent width, in Å (cf. Section 3.3.2).

Ia	Iab	Ib	II	III
< 3	3–4	4–5	5–10	10–15

In our SMC dataset, the Hγ equivalent widths at given B magnitude are smaller for A0 stars than for later A types. We applied the Galactic calibration to A2–A7 subtypes (thereby assigning supergiant luminosity classes to some rather faint stars – see Fig. 11), while treating A0 stars in the same way as B-type stars (Table 3).

3.4 Later types

The remaining 'late'-type spectra with radial velocities consistent with SMC membership were classified using the criteria listed by Evans & Howarth (2003). Briefly, F- and G-type spectra are characterized by increasing metal-line strength as the temperature decreases; for completeness, the criteria are included here in Table 2. A spectral sequence is shown in Figure 6.

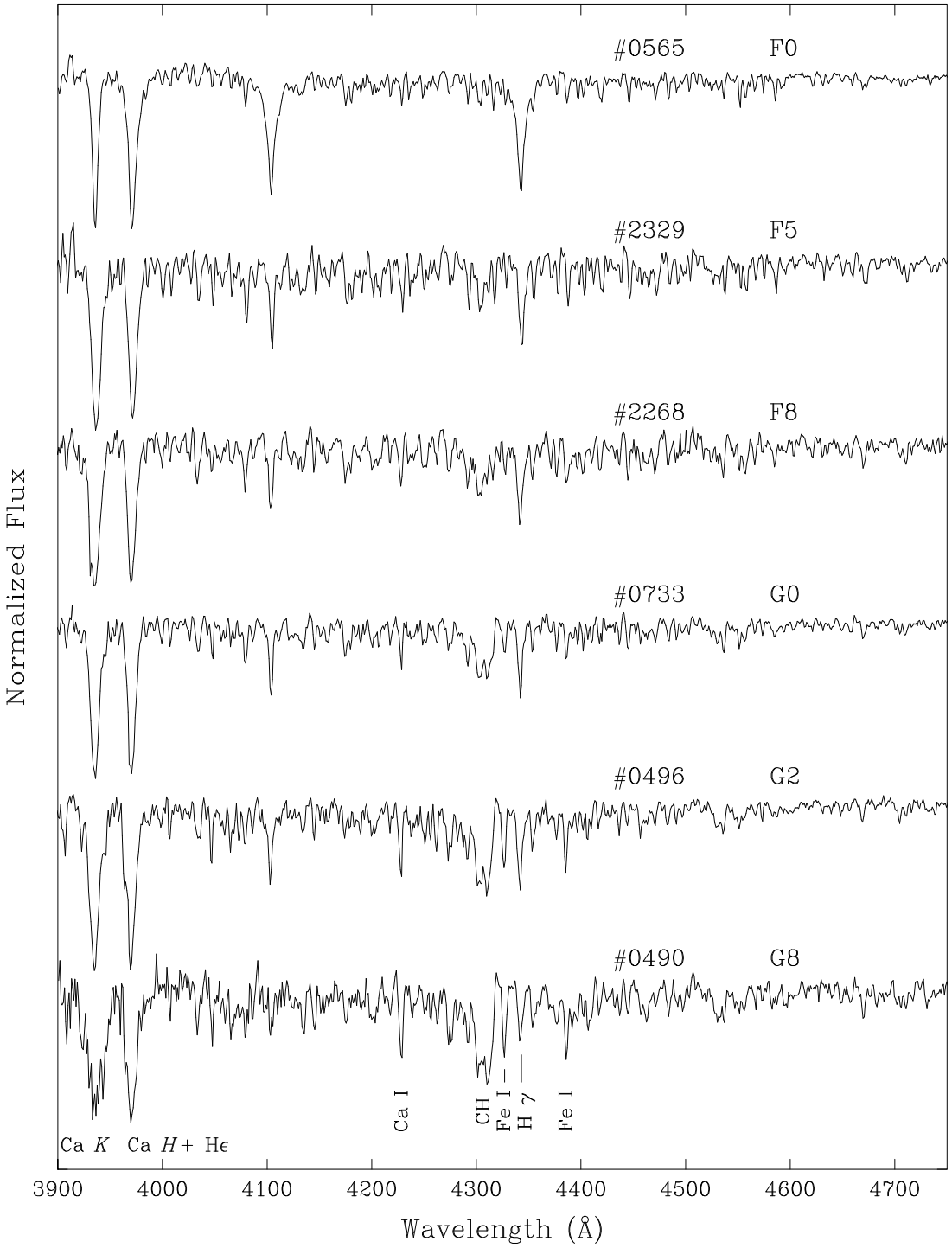

Figure 6. 2dF SMC spectra – V: F- and G-star spectral sequence. Stars are identified by 2dFS catalogue number. The spectral lines identified in 2dFS#0490 are Ca K (λ3933), the Ca H (λ3969) & Hϵ blend, Ca I λ4226, the CH G-band (around λ4300), Fe I $\lambda\lambda$4325, 4383, and Hγ. Successive spectra are vertically offset by one continuum unit.

Since our work is primarily concerned with the OBA domain, we have not explored luminosity-class diagnostics in later-type stars in the sample, though from their physical luminosities these objects are expected to be luminosity classes Ib–II for the most part.

4 CLASSIFICATION CHECKS

4.1 Comparison with other sources

Nine of the stars in the 2dF sample were observed by Lennon (1997). Lennon's are high-quality classifications, and pro-

Table 6. Comparisons of 2dF spectral types with those by Lennon (1997, first nine entries) and Massey et al. (1995). Parenthesised 2dF luminosity classes were assigned using the hybrid scheme described in Section 3.2.2.

2dFS #	AzV #	2dF	Other
0577	10	B2.5 (Iab)	B2.5 Ia
0801	96	B1.5 (Iab)	B1.5 Ia
1352	215	B0 (Ib)	BN0 Ia
1550	268	B2 (Ib)	B2.5 Iab
2174	404	B2.5 (Iab)	B2.5 Iab
2538	445	B5 (Iab)	B5 Iab
2773	462	B2 (Iab)	B1.5 Ia
2907	472	B2 (Iab)	B2 Ia
3235	490	O9.7 Ia+	O9.5 II
0668	28	B1-2 (II)	B1 I
0764	73	B0 (III)	O8.5 V
0786	84	B0.5 (IV)	B1 V
0836	114	O8 V	O7.5 V
1271	196	B1 (II)	B0.5 III
1324	209	B0.5 (IV)	B1 V
1357	217	B1-3 (II)	B1 III
1527	261	B2 (Ib)e	O8.5 I
1545	266	B1 (Iab)	B1 III
1550	268	B2 (Ib)	B2.5 V
1654	302	O9 III	O8.5 V
1741	326	B0 (IV)	O9 V
1759	328	B0 (III)	B0 V
1766	334	O9.5 III	O8.5 V
1858	346	B1-5 (II)	B2 V
1879	351	B1-2 (Ib)e	B0 V
1904	354	B1-3 (II)	B1.5 V
1972	376	B1-2 (Iab)	Be
2033	386	B1-2 (II)	B1.5 V
2102	395	B3 (II)e	B1 III
2139	402	O9.7 Iab	Be
2201	409	B0.5 (Ib)	Be
2319	423	B0 (II)	O9.5 V
2413	436	B0 (II)e	O7.5 Ve
2717	456	O9.5 Ib	O9.5 V
2720	457	B1-3 (II)e	Be
2905	471	B0 (III)	B0.5 V
3047	480	O4-7 Ve	Oe
3249	491	B1-3 (III)	O7 III:
3530	503	B0-5 (II)e	Be

vide an external check on the current work. Table 6 shows the 2dF types compared to Lennon's classifications. With the exception of AzV 490, both the spectral and luminosity types agree to within one subtype; the differences for AzV 490 are astrophysical (Section 7.7.3).

Table 6 also compares the 2dF spectral types with those given by Massey et al. (1995) for 30 stars in common. The differences in spectral types are again generally not larger than one subtype, exceptions being AzV 261, 436 and 491, where our types are significantly later. Re-examining the 2dF spectra of these stars (Fig. 7), we could not justify revising our results. Neither AzV 261 nor 491 shows He II in our data, and, while the two 2dF spectra of AzV 436 at our disposal have low signal-to-noise, He I λ4144 appears stronger than He II λ4200 in both, implying a type later than O9.

Massey (2002) presents a compilation of spectral classifications for 436 stars, drawn from a variety of sources (but omitting Lennon's work); of these, 230 have slit spectra, the remainder being objective-prism results. We have 2dF classifications for 158 stars from the full listing; comparison with the long-slit types shows agreement to within, normally, 1–2 subtypes. There are two notable exceptions, namely AzV 133 and 336 (2dFS#5060 and 1776). Garmany et al. (1987) classified AzV 133 as B0n+O8: with the comment that broad, possibly double lines of the Balmer series were seen; in the 2dF data (Fig. 7) the Balmer lines appear unremarkable, and we classify the spectrum as O6.5 V((f)). Massey (2002) gives the spectral type for AzV 336 as WN2+abs (cf. B2 (III) from the 2dF spectrum); the WN star is actually the separate object AzV 336A (see Massey & Duffy 2001).

4.2 Multiple Observations

Fifty targets were observed with 2dF in both 1998 and 1999. These spectra were classified entirely independently, and test the internal consistency of the classifications. In all instances the spectral types from the two seasons agree to within one spectral subtype at the appropriate classification resolution. The quality of the data is such that small differences are not unexpected, especially in cases where the line ratios are near the edges of the classification bins.

The long-slit spectra from 2001 provide a further consistency check. The spectral types again agree with the 2dF results to within one spectral subtype.

Overall, therefore, we believe that, notwithstanding the limitations of our data, in general our classifications are consistent to within a spectral subtype at the (sometimes coarse) classification bins adopted.

5 PHOTOMETRY AND ASTROMETRY

Initial construction of the 2dF input catalogue was necessarily performed using APM photographic photometry for colour–magnitude selection. Subsequently, three important catalogues of CCD-based photometry of stars in the SMC have been published: OGLE (Udalski et al. 1998), MCPS (Zaritsky et al. 2002) and Massey (2002). We have used these catalogues to refine and extend photometry for our targets, and to characterize the input material.

We sought positional matches between the 2dF catalogue and the photometric catalogues, initially by coincidence within a circle of radius 3″. We then adjusted the catalogue co-ordinates by the (subarcsecond) median offsets in RA and declination, and then sequentially reduced the adopted 'match' radius while further adjusting the offset as necessary. (Using the median rather than the mean offset ensured that this process converged in zero or one iteration.)

This comparison is limited to the main catalogue of 4054 2dF targets, as we have incomplete APM data for the supplementary UIT targets, for which OGLE astrometry was used for spectrograph configuration (cf. Harries et al. 2003).

5.1 OGLE

The final adopted 'coincidence' radius was 1.2″, generating 1395 matches, plus a further 290 duplicates (cp. 1461, 9108 at 5″). The duplicates were resolved by selecting the

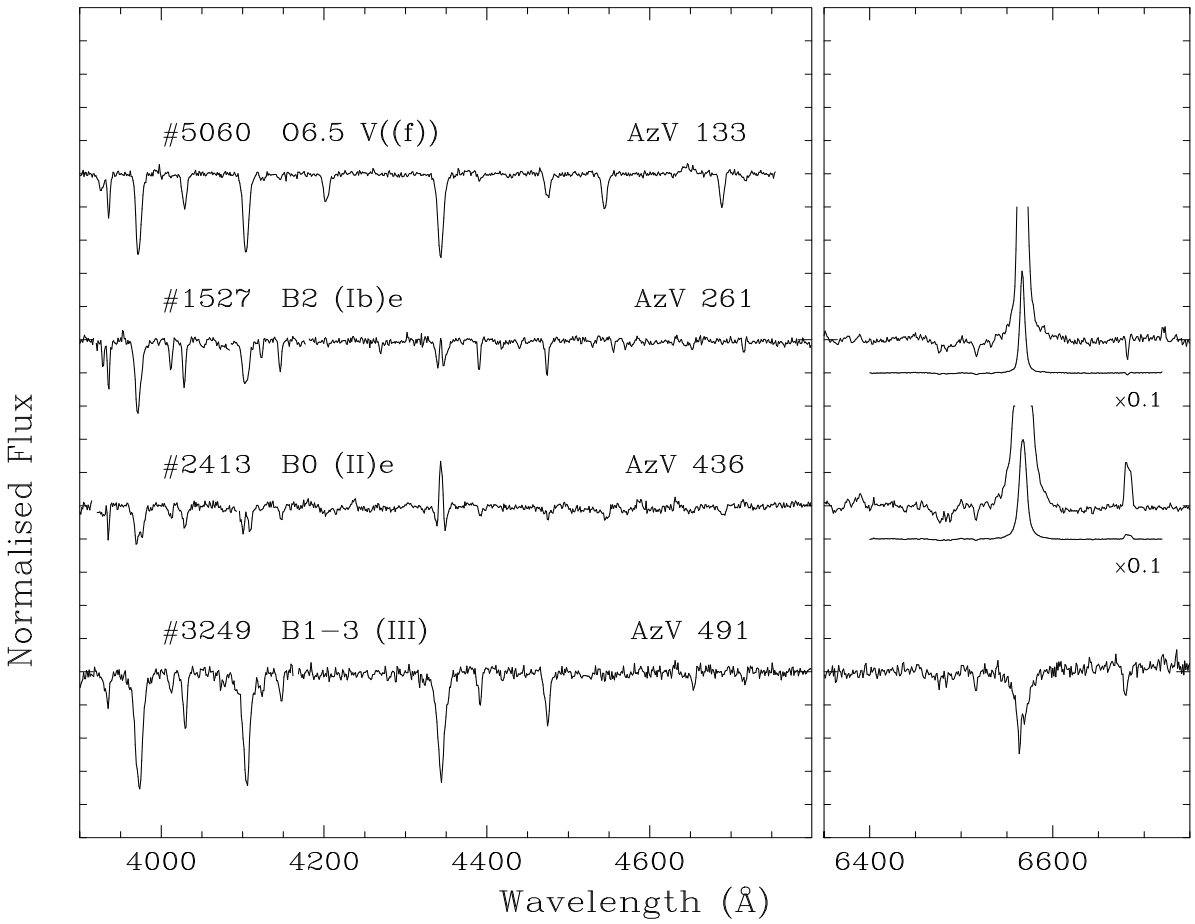

Figure 7. 2dF spectra for previously classified stars in the AzV catalogue (see Section 4.1 for details). Spectra are offset by 0.5 continuum units.

OGLE star closest in B magnitude to APM $B_{\rm J}$ (after applying the small zero-point correction to $B_{\rm J}$ discussed below). This proved very effective; spot checks of a few dozen duplicates showed that in every case there was one 'obvious' candidate (invariably the brightest OGLE star in the coincidence radius).

5.2 MCPS

The same procedures were adopted for the MCPS, with a $1.2''$ search radius yielding 3231 matches plus 67 duplicates, again resolved by magnitude matching. (Increasing to $5''$ adds a further 158 matches and 5797 duplicates.) This includes 15 stars where Massey photometry has been adopted for the MCPS (see Zaritsky et al. 2002).

5.3 Massey

Massey's survey was aimed at obtaining photometry for the brighter MC stars in particular. It has, accordingly, a brighter magnitude limit, allowing a larger plate scale than the other CCD-based surveys ($2.3''$/pixel vs. $\sim 0.7''$/pixel). Nonetheless, Massey's astrometry is sufficiently good that a $1.5''$ coincidence radius proved satisfactory, yielding 3115 matches, plus 47 duplicates (cp. 3211, 90 at $5''$).

We found that all the duplicates appear to be double entries in Massey's catalogue; we simply adopted results for the first entry. Further examination of this catalogue shows 4379 cases where two or more entries are spatially coincident to within $2.3''$ (3503 pairs with $\Delta B < 0.2$, 2694 with $\Delta B < 0.1$); 250 (183, 111) cases where three entries match; and 20 (13, 8) where 4 entries match. The mean B-band photometric offset for these coincidences is $0.00\pm0.27^{\rm m}$ ($0.00 \pm 0.08^{\rm m}$, $0.00 \pm 0.05^{\rm m}$), and the mean positional offset is $1.17 \pm 0.61''$ ($1.07 \pm 0.56''$, $1.03 \pm 0.55''$; all quoted errors are standard deviations), suggesting that $\sim$5% of objects in the catalogue may be the result of spurious multiple entries.

5.4 Adopted results

5.4.1 Astrometry

We conclude that the astrometry for all the datasets considered is internally consistent to better than $0.5''$ rms. The offsets between the APM astrometry and that from the photometric catalogues average $\Delta\alpha \simeq +0.4''$, $\Delta\delta < 0.1''$, APM minus other.[3] For reference, the APM sampling interval –

[3] The APM system currently available on-line has been transformed to the Tycho-2 system

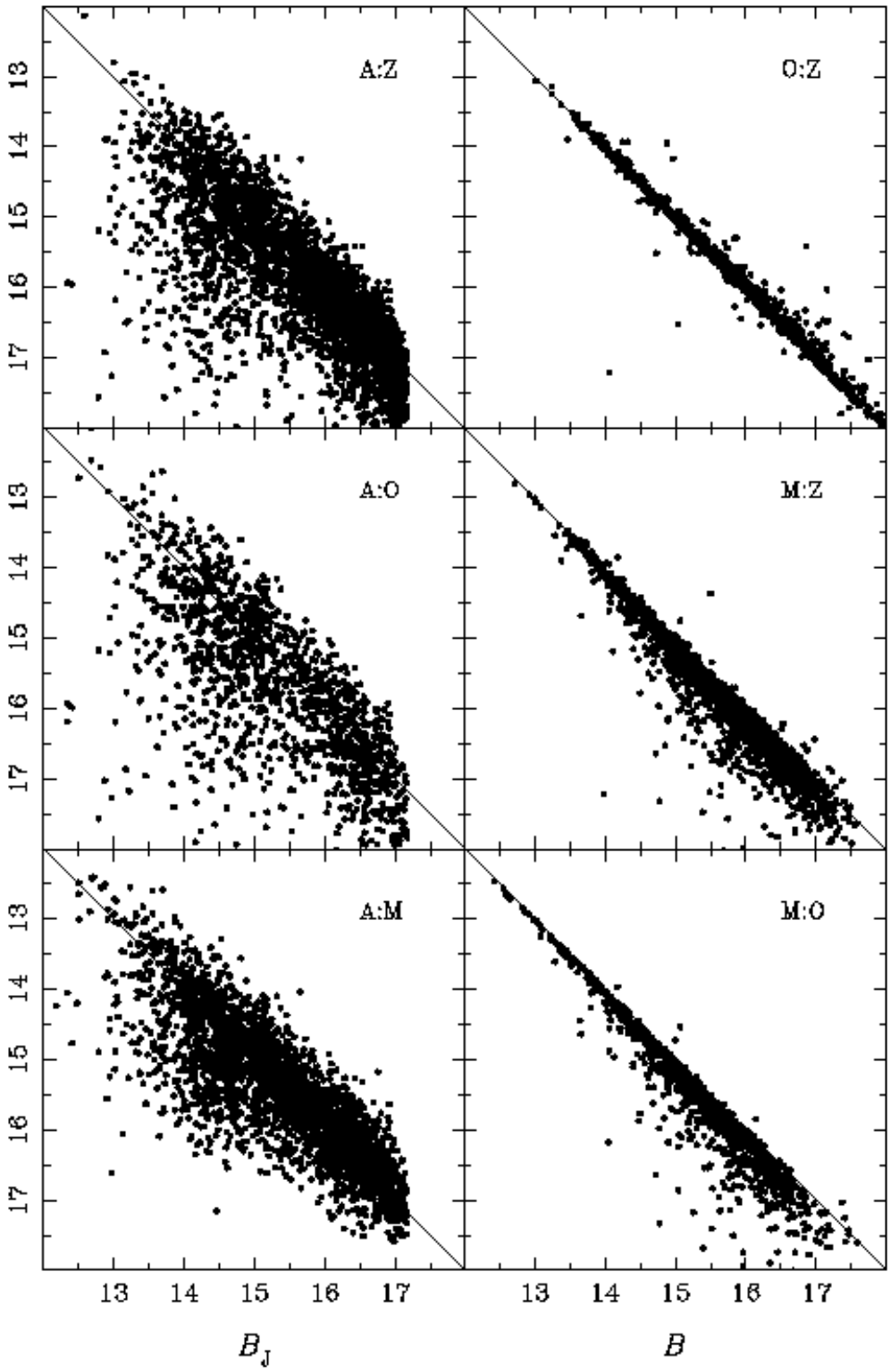

Figure 8. Comparisons of photometric results for stars in the 2dF survey, from APM, Massey, MCPS and OGLE (labelled A, M, Z and O, respectively, in this figure, with the x axis dataset listed first).

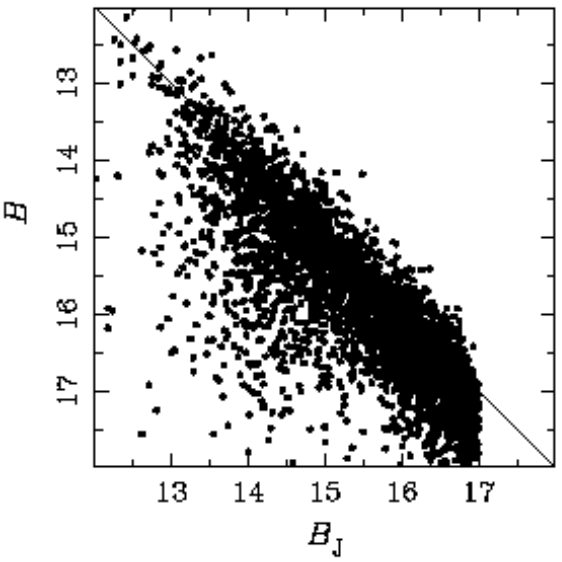

Figure 9. Comparison of input APM B_J photometry and adopted B photometry.

'pixel size' – is $0.5''$, and the 2dF fibres project to $2''$ diameter. We adopt the APM astrometry for the main 2dF catalogue.

5.4.2 Photometry

A comparison of photometric results for the stars in the spectroscopic survey is shown in Fig. 8. The distribution of APM photometric residuals is highly asymmetric for all reference catalogues, with an extended tail where the APM magnitudes are brighter than the comparison catalogue values. This asymmetry renders the arithmetic mean offset a statistic of limited utility; even the median is skewed by the moderately large fraction of these large residuals. The mode therefore gives the most meaningful average measure of the offsets for the APM photometry.

We made a small ($\mathcal{O}[0.1^{\rm m}]$) zero-point adjustment to the original B_J photometry to bring the modal offset from MCPS B to zero (colour terms being negligible). After this correction, the modal offset for OGLE is $-0.03^{\rm m}$ (APM fainter), and for Massey $-0.13^{\rm m}$. For matches within the 2dF sample, we also find median offsets MCPS−OGLE $= +0.02^{\rm m}$ (1265 stars, excluding those for which Massey photometry is substituted in the MCPS), MCPS−Massey $= +0.13^{\rm m}$ (2396), and OGLE−Massey $= +0.15^{\rm m}$ (1137). On the basis of these comparisons, we conclude that the APM B magnitudes have a zero-point uncertainty of order $0.1^{\rm m}$. Characterizing the (large) statistical uncertainty in the APM photometry in a useful way is complicated by the asymmetric nature of the distribution of magnitude differences. As an indicator, we find that 68% of matches have B-magnitude offsets in the range $\sim+0.6^{\rm m}/-0.4^{\rm m}$ of the mode.

The OGLE and MCPS results are in good mutual agreement, with Massey's results $\sim 0.1^{\rm m}$ brighter than OGLE/MCPS for this sample. (All three datasets are tied to Landolt (1992) standards.) Massey (2002) notes essentially the same offset in a comparison with traditional photoelectric photometry. For our present purposes, very precise photometry is not required, but for specificity (e.g., for diagrams), we generally adopted results from the multi-epoch, high-redundancy MCPS or OGLE surveys for preference (taking the better match to B_J where necessary, to minimise mismatches). The adopted main-catalogue photometry has 2513 values from MCPS, 747 from OGLE, 646 from Massey, and 147 from APM. The UIT-target photometry comes from MCPS and OGLE (97 and 10 stars, respectively). The complete list of cross-matches with photometric catalogues is given in Table A1 (Appendix A), available in full on-line, and a comparison of APM B_J magnitudes with adopted B magnitudes is made in Fig. 9.

6 THE RELATIONSHIP BETWEEN Hγ AND ABSOLUTE MAGNITUDE

6.1 Overview

Figures 10 and 11 show the relationship between Hγ equivalent widths, W_λ, and adopted B magnitudes, as a function of spectral subtype. As expected, there is a clear general trend of increasing W_λ with decreasing brightness, with $\partial W_\lambda/\partial B \simeq +1$Å$/^{\rm m}$ (for all BA subtypes, $B \simeq 13.5$–17.5). At $B \sim 14.5$, line strength increases slowly through the B spectral sequence, from ~ 2.5Å at B0–B3 to ~ 4.5Å at B9; $W_\lambda \simeq 7$–8Å for all A subtypes, excepting the transitional subtype A0, where $W_\lambda \simeq 6$Å (with considerable scatter), and A7, where there is a suggestion that W_λ starts to fall off. These results are in general agreement with previous work (Hutchings 1966; Balona & Crampton 1974; Azzopardi 1987), though based on better-sampled, higher-quality material. The exception to this generalization is that W_λ begins to decline at A7/F0 in our data, whereas Azzopardi (1987) finds monotonically increasing W_λ from early B through early F subtypes, with $W_\lambda \simeq 8$Å at F0 Ib (at $B \simeq 15$).

The insensitivity of W_λ to A spectral subtype, throughout the magnitude range we sample, provides justification for the subtype-independent luminosity classification scheme adopted in Section 3.3.2 (although Hγ equivalent widths are more strongly subtype dependent at fainter luminosity classes).

6.2 The dispersion

There is significant scatter in the equivalent widths at a given subtype and magnitude. Observational errors could contribute to this scatter in several ways, including photometric errors, equivalent-width errors, and classification errors.

6.2.1 Photometric errors?

Although the formal photometric uncertainties in the CCD data are generally negligible compared with the observed dispersion, arbitrarily large errors can be introduced if the photometric catalogue star is mismatched with the spectroscopic catalogue entry. As we have shown, the APM photometry is also subject to relatively large uncertainties. To investigate these issues we examined the residual datasets

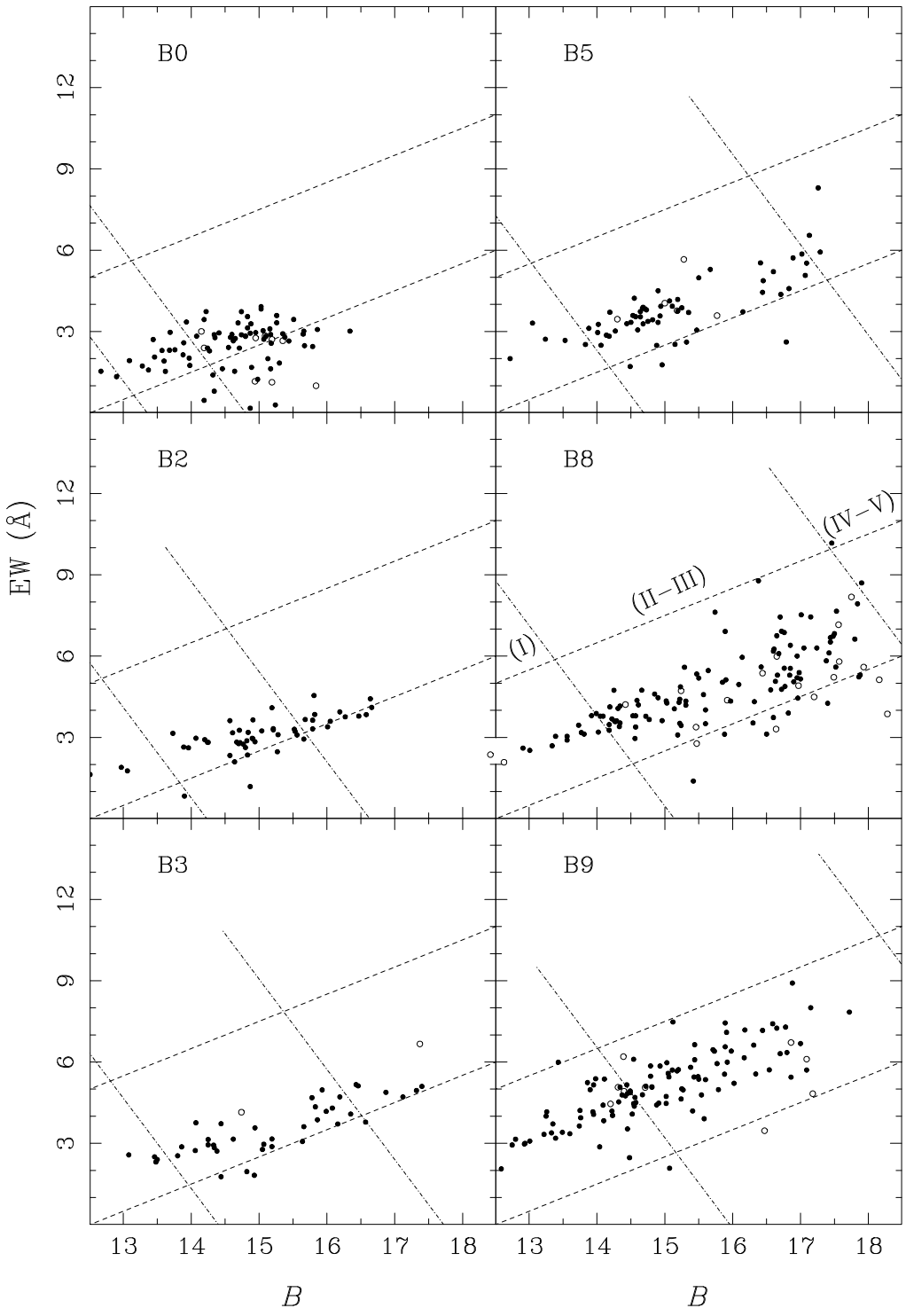

Figure 10. Hγ equivalent width as a function of B magnitude for B stars in the 2dF spectroscopic catalogue. Only stars with 'precise' classifications (uncertainty ±1 subtype) are shown. The diagonal lines of constant $(B - \mathrm{W}_\lambda)$ (running lower left to upper right) are intended solely to provide a point of reference for the reader, and have no physical significance; the lines of constant $(B + 0.3\mathrm{W}_\lambda)$ show the adopted boundaries between supergiants (luminosity class Ib and brighter), giants (II and III), and main-sequence (IV and V) stars. The open circles show stars for which we have only APM photometry, or for which the CCD results differ by more than 1^{m} from APM measurements (cf. Section 6.2.1). The brightest B8 star shown (just outside the main data frame) is AzV 72, which has previously been noted as a member of the class of SMC supergiants supposedly having anomalously strong hydrogen lines. It appears unexceptional in our dataset (cf. Section 7.5).

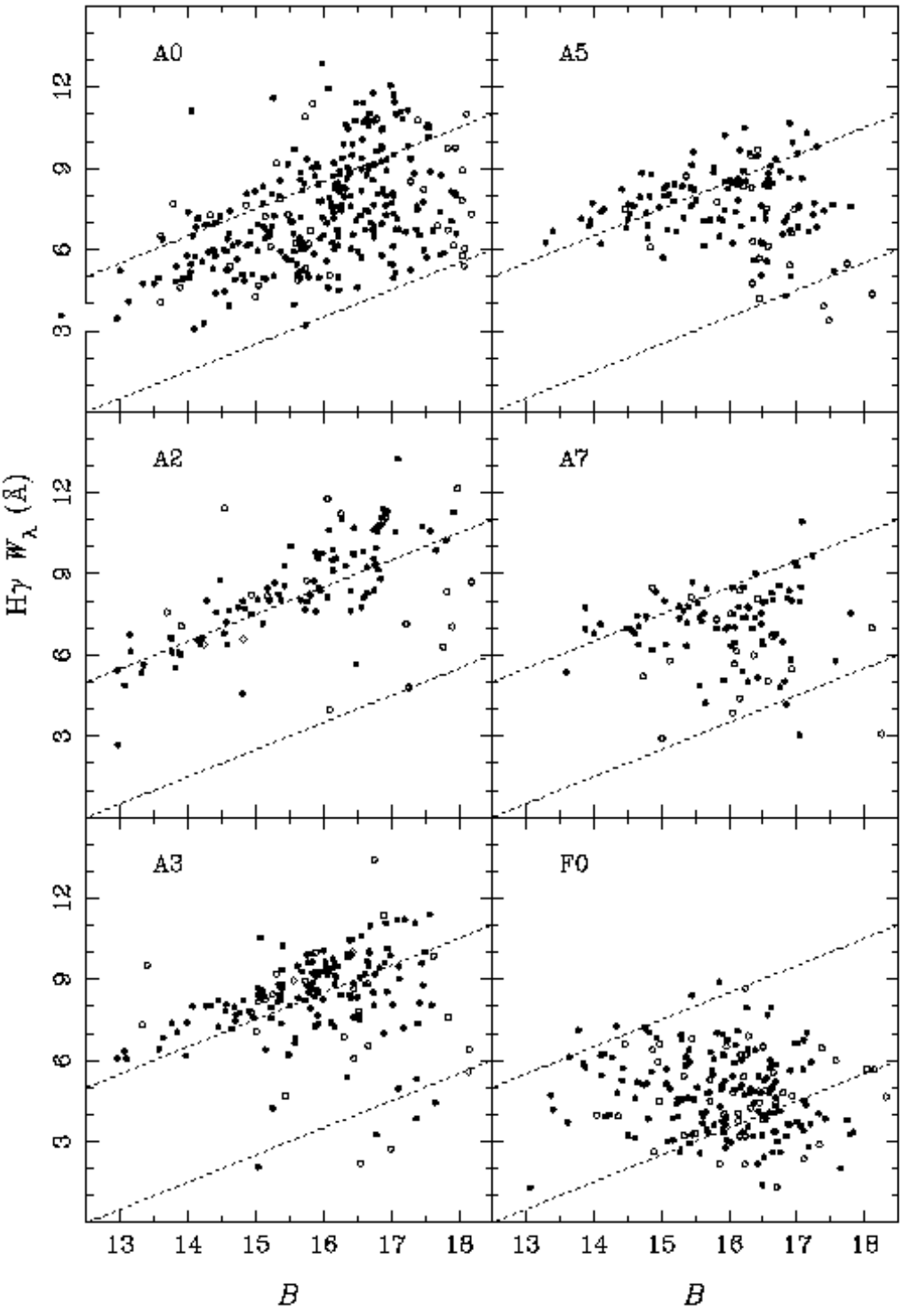

Figure 11. Hγ equivalent width as a function of B magnitude for A stars in the 2dF spectroscopic catalogue. Only stars with 'precise' classifications (uncertainty ±1 subtype) are shown. The diagonal dotted lines of constant $(B - W_\lambda)$ are intended solely to provide a point of reference for the reader, and have no physical significance. The open circles show stars for which we have only APM photometry, or for which the CCD results differ by more than 1^m from APM measurements (cf. Section 6.2.1). The brightest A0 star shown (just outside the main data frame) is Sk 1, which has previously been noted as a member of the class of SMC supergiants supposedly having anomalously strong hydrogen lines. It appears unexceptional in our dataset (cf. Section 7.5).

after exclusion of data for which the CCD results differ from the APM photometry by $1^{\rm m}$ or more (thereby reducing the probability of cross-catalogue mismatches), or for which we have only APM photometry. Excluding these arguably questionable data reduces the scatter slightly, but the dispersion is large even for the remaining CCD results (Figs. 10 and 11).

6.2.2 Equivalent-width errors?

Because the sky backgrounds in the 2dF spectra are not determined directly, but are scaled from separate sky fibres, the accuracy of background subtraction (and hence equivalent widths) is a source of concern. In practice, the continuum sky background (typically, equivalent to a $\sim 20^{\rm m}$ star at B) is unlikely to exceed $\sim$10% of the gross signal, even in relatively poor cases. Nonetheless, to check this point we made measurements on the conventional long-slit spectra described in Section 2.4. The comparison of equivalent widths is made in Fig. 12; agreement is good (although the comparison is limited to relatively bright stars).

A small number of the brightest stars in our 2dF survey are in common with the Azzopardi (1987) survey of Hγ line strengths in SMC supergiants. We compare our equivalent widths with his in Fig. 12. Agreement is generally acceptable, excepting three outliers, for which our equivalent widths are noticeably greater than his. Two of those three outliers were included in the long-slit observations (cf. Fig. 12), and our measurements suggest that it is the newer data that are the more reliable. (Azzopardi's measurements were made on photographic objective-prism spectra obtained with a resolving power perhaps half that of the 2dF observations.)

Although the evidence therefore suggests that our measurements are generally satisfactory, the tendency for some equivalent widths to appear 'too small' (Figs. 10 and 11) does leave open the possibilities that Hγ may, in those cases, be contaminated by nebular emission at a level too small to be obvious at our resolution, or that an overcorrection for the background signal has been applied. The former issue is partially addressed by the identification in Table A1 of stars associated with catalogued nebulosities, and by scrutiny of the Balmer-line spectra (Section 7.1); and the latter by the preceding discussion.

6.2.3 Classification errors?

Since the mean equivalent width of Hγ varies as a function of spectral subtype at given B magnitude, errors in subtype assignments could introduce scatter. The scatter is noticeably large at spectral type A0, where the rate of change of W_λ with spectral type is greatest. Late-B stars have significantly smaller equivalent widths, on average, than the early-A stars, so late-B stars misclassified as early-A stars could explain the tail of 'low-W_λ' A0 stars.

To investigate this further, and more generally, we measured the ratio of Ca K to Hϵ+Ca H using a simple constrained gaussian fit. The equivalent-width ratio[4] is plotted against Hγ equivalent width in Fig. 13. There is very good separation between A- and B-type stars, *except* for the A0 stars, which in this plane are mingled with both earlier and later types. In effect, for both B-type and A0 stars the K/H ratio is just 'small', while the Hγ equivalent width is influenced by luminosity as much as by temperature.

The primary criterion for resolving the B9/A0 ambiguity is the presence of He I λ4471 in the earlier type. A plausible explanation of the scatter in W_λ, at A0 in particular, is, therefore, that B9 spectra have been misclassified in poor-quality spectra with S/N too low to allow the helium line (weak at this subtype) to be identified. An attempt to improve A0–B9 separation using automated measurements of 4471/4481 proved fruitless, because of the low S/N of the data. Outliers in the W_λ–B plane were therefore identified and the spectra re-inspected for evidence of any anomalies. For the earlier spectral types, an anomalous position in this plane correlates with Balmer-line emission (stellar or nebular); and at later types, stars with emission are also displaced. However, most mid- to late-A outliers appear unexceptional (other than in respect of their Balmer-line weakness) at our dispersion and signal-to-noise.

A further possibility is that unresolved companions may cause or exacerbate the spread in the W_λ–B plane. This must be a factor at some level, but comparison of the Hγ equivalent widths (at a given spectral type) for cluster members and field stars reveals no greater dispersion for the former, such as might be expected if blends were important. Furthermore, any close binary companions to BA giants and supergiants are not expected to be significant contaminators of the optical spectra, in general. We conclude that the dispersion in W_λ most probably arises primarily from a combination of measurement errors, unresolved nebular emission, and minor classification errors, with astrophysical effects (such as multiplicity and intrinsic emission) as secondary contributors.

7 OBJECTS OF SPECIAL INTEREST

7.1 Balmer-emission statistics

The blue-region spectra at our disposal are, for the most part, inadequate to distinguish reliably between any intrinsic narrow Balmer emission and nebular emission. Nonetheless, in a number of cases resolved or structured Balmer emission is identifiable. As a rough guide to objects likely to be of interest, we therefore categorized all observed Balmer lines as showing absorption; narrow (i.e., unresolved, probably nebular) emission; resolved emission; double-peaked emission; or P-Cygni profiles.

Stars were categorized rather conservatively (i.e., only reasonably definite cases were categorized as 'resolved' rather than 'narrow', or as 'double' rather than 'resolved'). Each Balmer line was categorized independently for each star (4161 targets have Hγ observed, 2095 Hβ, and 1091 Hα). After reviewing a handful of anomalies (and consequently revising Hγ 'r?' to 'n'), all stars having red spectra and showing intrinsic Hβ emission (or suspected intrinsic

[4] This quantity is closely related to, but not the same as, the K/H ratio used in the visual classifications. There is reasonable, though not perfect, separation of individual A subtypes in this plane.

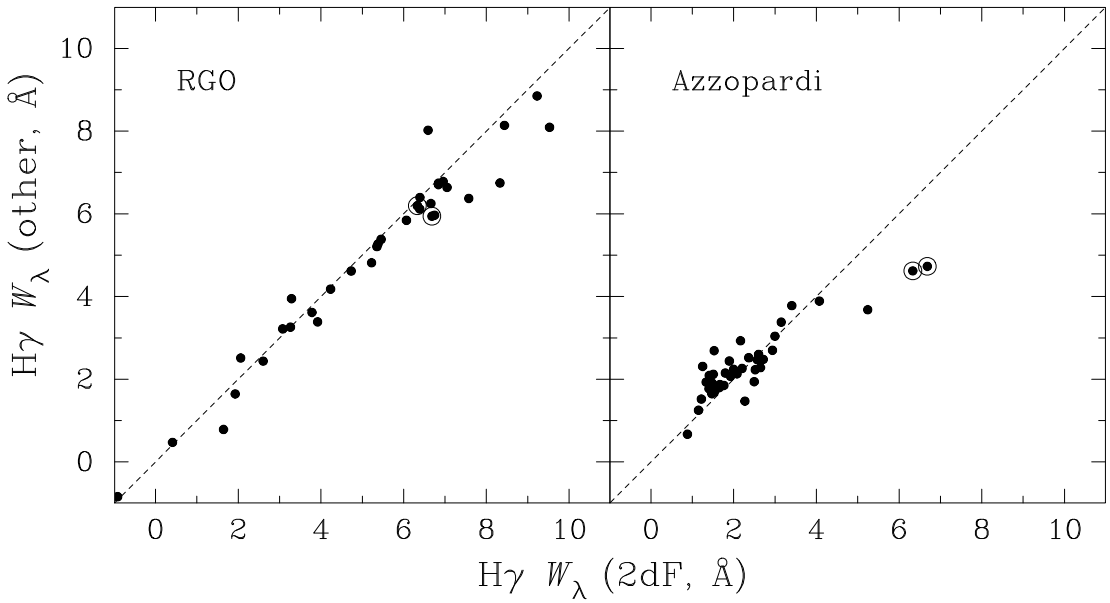

Figure 12. Comparison of Hγ equivalent widths measured in 2dF and RGO spectra, and by Azzopardi (1987). The circled points in each panel show measurements for the same two stars, AzV 401 and 431; the agreement between 2dF and RGO measurements suggest that it is Azzopardi's measurements that are discrepant for these two stars.

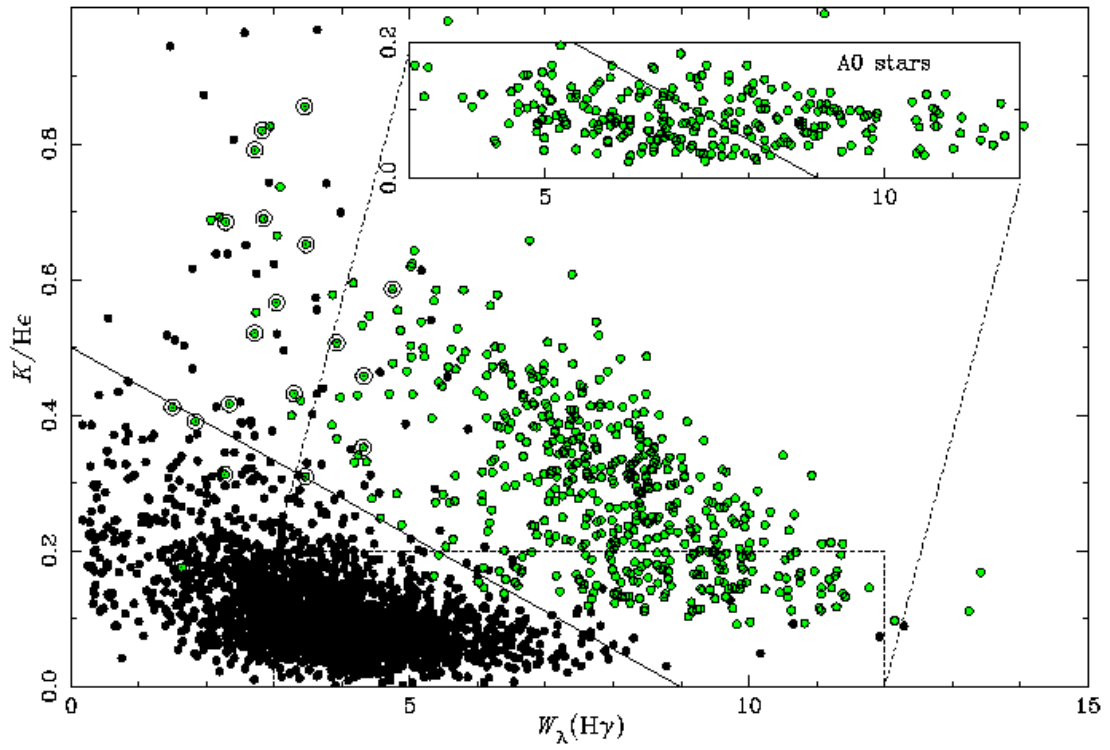

Figure 13. Ratio of Ca K to Hε+Ca H as a function of Hγ equivalent width (in Å). The diagonal line is drawn 'by hand' to separate stars classified as B (solid black circles, lower left) from those classified as A2–A7; these two groups are well separated in this plane. The displaced inset shows the A0 stars. The circled points are the possible 'composite-spectrum' stars (Section 7.4).

Table 7. Numbers of stars by spectral type from the APM- and UIT-selected samples. In the latter case, totals are given for both the pure UIT-selected sample and (in square brackets) other UIT targets which were matched in the 2dF catalogue. 'Em' lists the percentage of stars that show emission at Hα in each spectral bin (Section 7.1). 'AF' is used for the possible 'composite-spectrum' stars (Section 7.4).

Spectral	APM		UIT				Total	Em.
Type	N	%	N	%	N	%	N	%
O+W	121+1	3	18	17	[21+1]	6	139+1	20
B<5	2454	61	72	67	[274]	79	2526	26
B≥5	327	8	9	8	[30]	9	336	14
A<5	593	15	7	7	[17]	5	600	2
A≥5(+'AF')	233+19	6	0+1	1	[1+2]	0	223+20	4
FG	306	8	0	0	[1]	1	306	0
Total	4054		107		347		4161	

emission) also show Hα emission, and all stars showing intrinsic Hγ emission show Hβ and Hα emission, where data exist.

A hundred and ninety-seven stars with usable red-region 2dF spectra (18%) show intrinsic Hα emission of some sort; 161 stars with Hβ spectra (8%) show Hβ emission; and 154 stars (4%) show Hγ emission. The targets for the red-region spectra were biassed towards objects with 'interesting' blue spectra; correcting for this bias, ∼14% of stars in the input catalogue show Hα emission. To a good approximation, in our data Hα is twice as effective as Hβ in disclosing intrinsic Balmer emission, and Hγ half as effective.

In the majority of cases (∼80%), blue-region Balmer emission consists of resolved (or marginally resolved), undisplaced (or only moderately displaced) narrow emission, without obvious emission in any other lines. Emission features in the Hα spectra are invariably substantially broader, or clearly structured. Table 7 includes a summary of the distribution of Balmer emission by spectral type, peaking at early B.

7.2 Be-type spectra

BA stars reliably exhibiting double-peaked emission in at least one Balmer line (or suspected double-peaked Hβ accompanied by Hα emission) are listed in Table 8, and illustrative spectra are shown in Fig. 14. The stars with double-peaked emission show a spread in absolute magnitude from $M(B) \simeq -5$ to the cutoff of our survey ($M(B) \simeq -1$), with a mode of about $M(B) \simeq -3$, and are classified (usually rather coarsely) as early B, and so are likely to represent the bright tail of the distribution of classical Be stars, if we adopt the *Hipparcos*-based absolute-magnitude scale for Galactic Be stars given by Wegner (2000). Because of their relative brightness, these 2dF stars are attractive targets for, e.g., investigation of short-term line-profile variability (cf. Baade et al. 2002).

Encouraged by our referee, we have also listed stars whose spectra display single-peaked, resolved emission at either Hα or Hβ as 'Be'-type in Table A1. Many or most of these stars may be classical Be stars, but our primary motivation in adding the 'e' suffix to the catalogue spectral types is to alert users to the qualifying supplementary emission-line information.

None of the stars in Table 8 have been explicitly identified as Be stars in the literature, but several other previously known objects are included in the 2dF catalogue: one from the sample of Be stars studied by Hummel et al. (1999), 2dFS#1115 (NGC 330 KWB Be 258, Grebel 9), and a further four potential Be stars listed by Keller, Wood & Bessell (1999): 2dFS#1077=KWB Be 278; #1087=522; #1277=122; and #1326=355. Of these five stars, 2dFS#1077 and #1277 show marginally resolved (i.e., broadened) emission at Hγ (only 2dFS#1326 has Hβ observed), while 2dFS#1277 and #1326 have red spectra, both showing strong, single-peaked Hα emission.

7.3 B[e] stars

2dFS#2837 has previously been catalogued as LHA 115-N82, Lin 495, and MA93-1750 (Henize 1956; Lindsay 1961; Meyssonnier & Azzopardi 1993), and was reported as a B[e] star by Heydari-Malayeri (1990). It is the only previously reported B[e] star in our sample. We observed it in 1998 with 2dF, and again in 2001 with the RGO spectrograph. The two spectra are indistinguishable (the RGO spectrum is shown in Fig. 17), and similar to that shown by Heydari-Malayeri if allowance is made for the differences in resolution.

The only other star in the 2dF dataset that shows similiarities to #2837, and in particular the same Fe [II] emission lines, is 2dFS#1804. Unfortunately, we have only a single, blue-region, observation of this star (Fig. 17), but, like #2837, it has been repeatedly catalogued as an Hα emission object: LHA115-S38, Lin 418, MA93-1405 (Henize 1956; Lindsay 1961; Meyssonnier & Azzopardi 1993). This relatively bright star ($B \simeq 14.0$) is clearly worthy of further study.

7.4 Composite-spectrum targets

Our examination of eighteen of the 2dF spectra indicated an ∼A-type classification from Ca K, while other metal lines (including the G band) suggested spectral type ∼F. These targets form a distinct group in the SMC survey; the spectra are superficially suggestive of Galactic Am stars in several cases, but classical Am stars would be too faint to feature in our survey. Our targets are unlikely to be foreground objects, both because of the observed radial velocities and because the surface density is implausibly high. We also provisionally rule out contamination by the solar (i.e., twilight or bright-moon) spectrum; most of these stars were observed in dark skies when the moon was below the horizon (and similar features are not seen in any B-star targets).

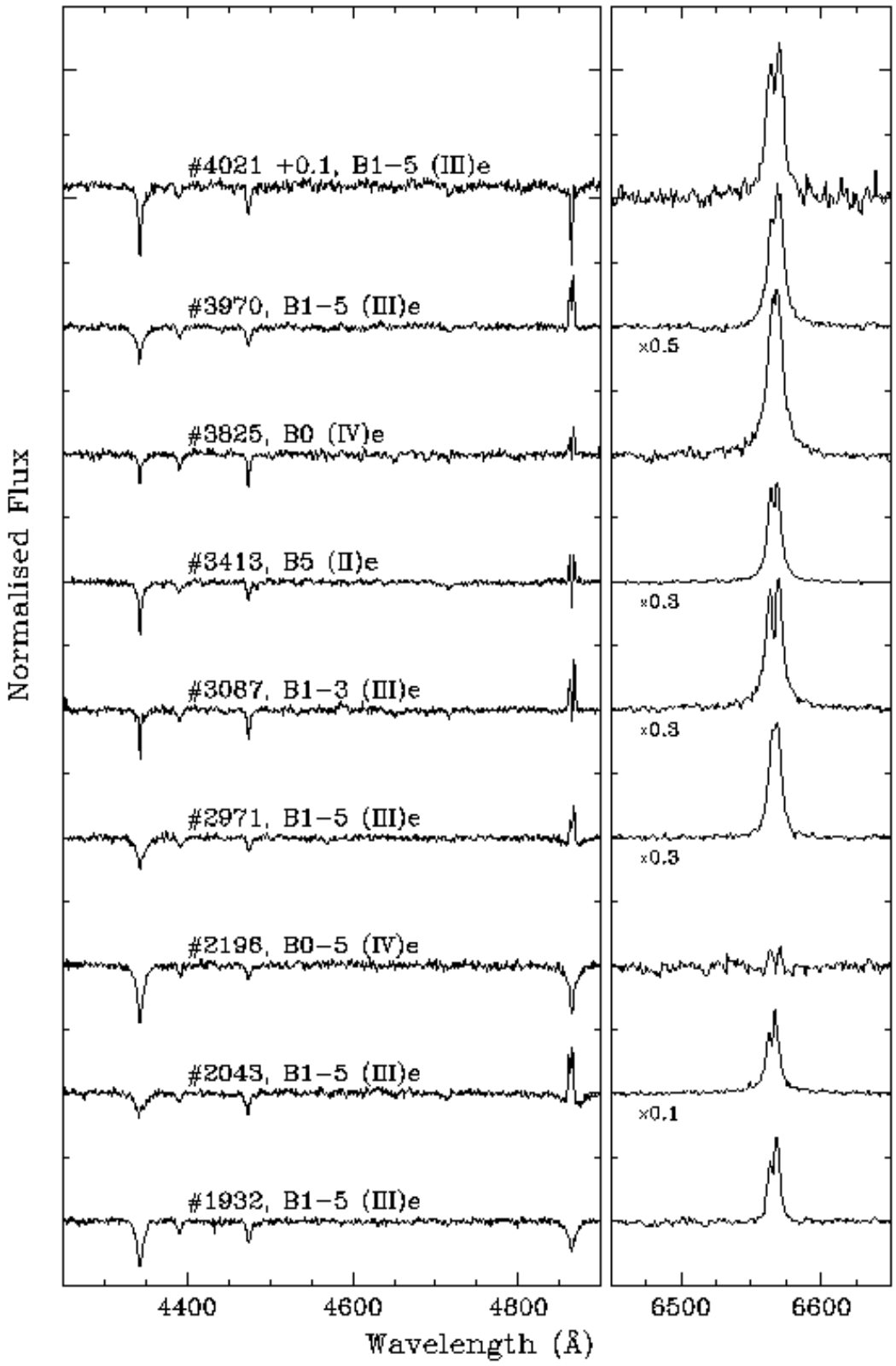

Figure 14. Spectra of selected Be stars. Each spectrum is vertically offset by 1.0 continuum units. The luminosity classes assigned to these stars should be regarded with caution, as Balmer-line emission is liable to result in a 'too bright' classification with our 'hybrid' methodology (Section 3.2.2).

Table 8. Presumed classical Be stars: B stars showing double-peaked emission in the Balmer lines. The last three columns encode the spectral appearance in Hγ, Hβ, and Hα. Here 'a' means absorption, 'n' means narrow (possibly nebular) emission, 'r' means resolved (though narrow) emission, 'd' means double-peaked emission, and 'e' means broad single-peaked emission. The luminosity classes assigned to these stars should be regarded with caution, as Balmer-line emission is likely to result in a 'too bright' classification with our 'hybrid' methodology (Section 3.2.2).

2dFS	Other	B	Sp.	Balmer		
0080		17.18	B0–5 (V)e	γa	βd	
0113		15.64	B1–2 (III)e	γa	βd	
0306		14.35	B0–5 (II)e	γa?	βd	
0922		16.00	B0–5 (V)e	γd?	βd	
1306		16.62	B0–5 (IV)e	γa		αd
1496	MA93-1216	15.77	B0.5 (V)e	γd?		αe
1551		16.51	B0–5 (IV)e	γa		αd
1558		17.44	B0–5 (V)e	γa	βd	
1932	MA93-1490	15.32	B1–5 (III)e	γa	βa	αd
2043	MA93-1539	15.99	B1–5 (III)e	γa	βd	αd
2196		16.21	B0–5 (IV)e	γa	βa	αd
2267	MA93-1621	15.84	B1–5 (III)e	γd?		αd
2316	AzV 422, MA93-1637	13.97	B1–5 (II)e	γa	βd	
2360		16.96	B0–5 (V)e	γa	βd	
2598	MA93-1707	16.25	B1–5 (III)e	γa		αd
2613	MA93-1711	15.65	B0–5 (III)e	γa	βd?	αd
2786		17.53	B1–5 (V)e	γa		αd
2794		15.02	B1–5 (II)e	γa	βa	αd
2802		15.66	B0–5 (III)e	γn	βr	αd
2971	MA93-1775	15.83	B1–5 (III)e	γa	βd	αe
2986		15.07	B1–3 (III)e	γa	βa	αd
3087	MA93-1813	15.78	B1–3 (III)e	γd	βd	αd
3325		16.07	B0–5 (IV)e	γa		αd
3413	MA93-1868	14.96	B5 (II)e	γa	βd	αd
3426	MA93-1871	16.15	B0–5 (III)e	γa	βd	
3436		15.93	B1–5 (III)e	γa	βd?	αd
3479	MA93-1881	15.82	B1–5 (III)e	γa		αd
3512	MA93-1886	14.82	B3 (II)e	γa		αd
3573	MA93-1894	15.88	B1–3 (III)e	γr		αd
3628		14.67	B1–3 (II)e	γd?		αe
3716		14.97	B1–5 (II)e	γa		αd
3730		16.99	B0–5 (V)e	γd?	βd	
3795		15.15	B1–3 (III)e	γr?		αd
3825		15.19	B0 (IV)e	γa	βd	αe
3928		15.36	B1–5 (II)e	γd?	βd	
3970		15.48	B1–5 (III)e	γa	βd	αd
3998		15.49	B0–5 (III)e	γa		αd
4021		15.49	B1–5 (III)e	γa	βd?	αd

We conclude that many of these observations may represent composite spectra. The rate of incidence is $\mathcal{O}(1\%)$, similar to Galactic values, but these cannot be exact counterparts of Galactic composite-spectrum systems, which typically consist of a near-main-sequence A star with a G giant; our targets are somewhat more luminous. They are, however, 'too blue' in $(U-B)$ and/or 'too red' in $(B-V)$ for the most part (Fig. 15), consistent with a generic composite-spectrum intepretation. Unfortunately, the photometric anomalies are not sufficiently clear-cut for these stars to be uniquely or unambiguously identifiable from colours alone. In the H/K plane (Fig. 13) these stars are also outliers, falling at the small W$_\lambda$(Hγ) end of the A-star distribution (which could, however, be construed as a consequence of incorrect background subtraction).

R.O. Gray has extensive experience with spectral classification in the relevant part of the HRD (e.g., Gray et al. 2001), and very kindly volunteered to examine some of these spectra. He was able to re-interpret three of the targets as having spectra similar to normal or near-normal Galactic F-type stars, within bounds of the data quality (although the radial velocities argue against this interpretation), but confirmed apparent abnormalities in several other cases. We have no repeat spectroscopy for any of these stars, and so are unable to rule out some instrumental, rather than astrophysical, peculiarity; attempts to obtain new spectra were thwarted by bad weather. Good-quality, long-slit spectra of just one or two of these targets could go a long way towards clarifying their true nature.

7.5 The 'Anomalous A supergiants'

Following earlier work on LMC stars by Sanduleak (1972) and Fehrenbach & Duflot (1972), Azzopardi (1982) and

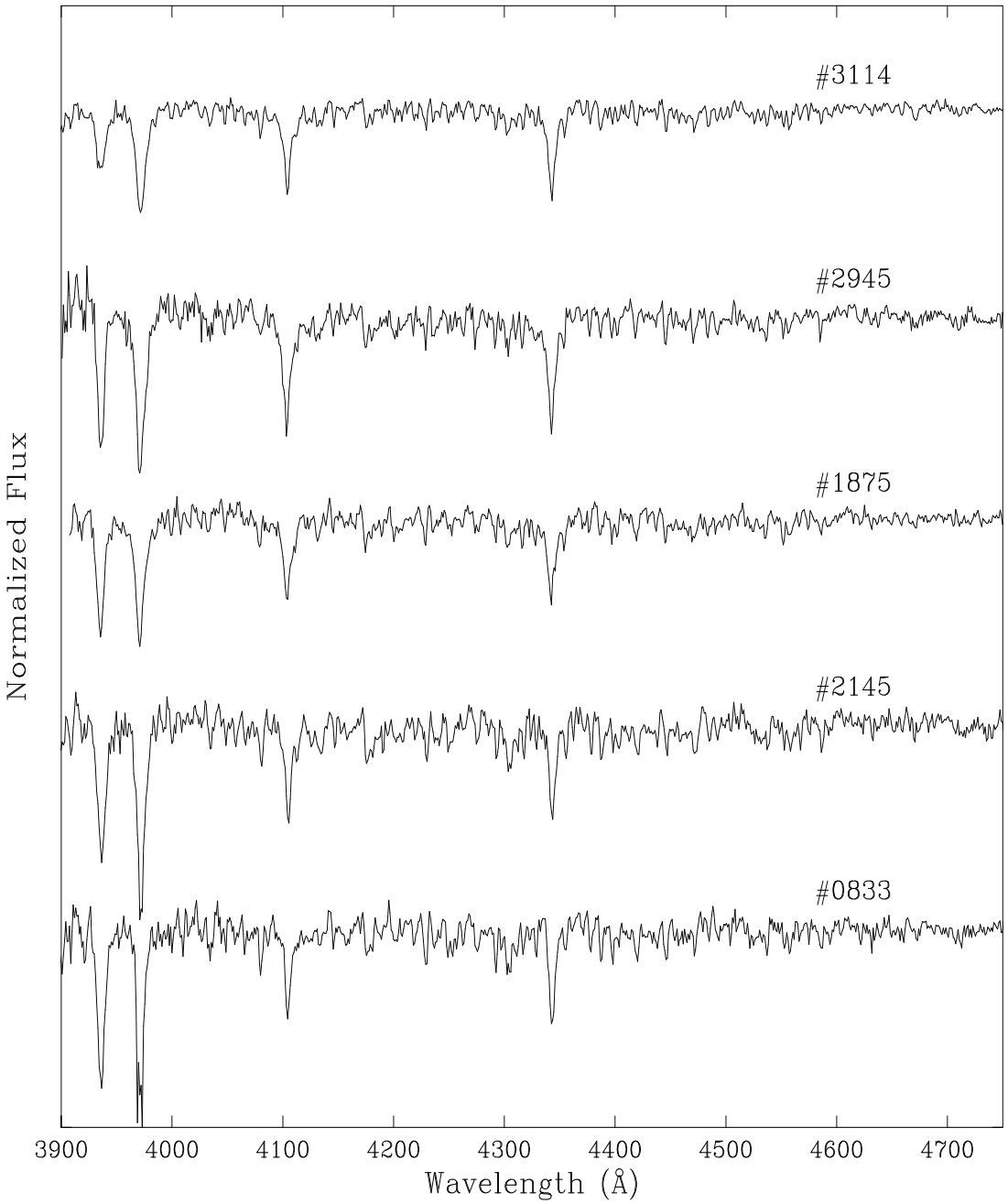

Figure 16. 2dF SMC spectra – VI: Examples of possible composite-spectrum targets. Stars are identified by 2dFS catalogue number. Successive spectra are vertically offset by one continuum unit.

Humphreys (1983) noted a population of 'anomalous A-type supergiants' in the SMC, characterized by unusually large Balmer-line strengths and red $(U-B)$ colours. In our sample (for which the great majority of targets are substantially fainter and less luminous that those studied by Azzopardi and by Humphreys) there is very little evidence for any stars having these characteristics (cf. Figs. 10, 11, and 15).

We have only two targets among those listed by Humphreys (1983, her Table 1C) as anomalous: Sk 1 (2dFS#0109) and AzV 72 (Sk 37, 2dFS#0765). Our classifications (A0 (Ia) and B8 (Iab), respectively) are in excellent agreement with hers (A0 I and B8 I), but neither star is exceptional in the W_λ–B plane in the context of our dataset[5] (Figs 10 and 11). This is consistent with an unpublished study by E.L. Fitzpatrick (personal communication),

[5] For AzV 72 we have only APM photometry: $B = 12.43$. Azzopardi & Vigneau (1975) and Ardeberg (1980) report concordant UBV measurements giving a somewhat fainter $B \simeq 12.88$, strengthening the normality of this star in the W_λ–B plane.

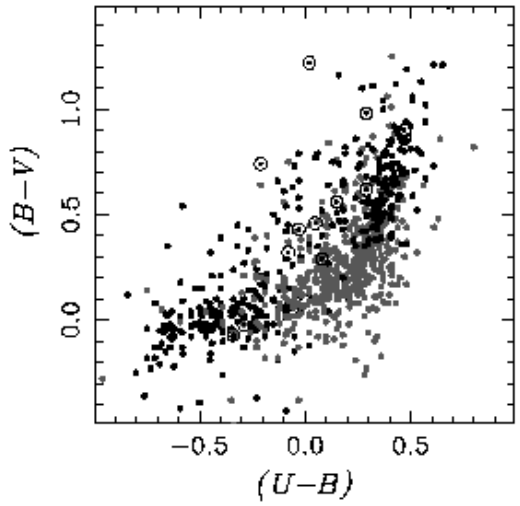

Figure 15. The two-colour diagram for late-B, A, and F stars, based on photometry from Massey (2002). The possible 'composite-spectrum' stars (Section 7.4) are shown as circled dots, and apparently normal A stars in a different shade to the BF stars.

in which he argues, persuasively in our view, that many reported anomalies in Magellanic Cloud A supergiants can be attributed to the lack of a proper reference framework of *normal* stars at Cloud metallicities (cf. Lennon 1997 for a related critique of metal-line luminosity classification of SMC B-type supergiants).

Humphreys, Kudritzki & Groth (1991) proposed a physical explanation for the strength of the Balmer lines in the supposedly anomalous stars. They suggested that these stars are post-red-supergiants, with enhanced surface helium abundances leading to increased atmospheric pressure at given temperature. By itself, this is a plausible argument, but standard evolutionary models suggest that post-red-supergiant BA supergiants should have around half the mass of pre-red-supergiants at the same luminosity and $T_{\rm eff}$. The reduction in $\log g$ would be expected to lead to *reduced* Balmer-line strengths (which may be a contributory factor to the small-W$_\lambda$ stars in our sample).

7.6 The UIT targets

Classifications for the 107 UIT-selected targets are summarised in Table 7. As for the main catalogue, roughly three-quarters of the sample are B-type stars, but the UV-selected sample is uncontaminated by FG stars, and features a much smaller proportion of A-type stars than the APM, $(B-R)$-selected sample. We also searched the main APM catalogue for UIT stars. There are 347 matches with separations of less than 2″ (cp. 386 for 5″, 223 for 1.2″), and the distribution of spectral types closely matches that of the UIT-selected sample (Table 7), albeit with somewhat smaller fraction of O stars.

Parker (2002) discusses whether there was a hitherto undiscovered population of early-type field stars in the Clouds, well away from obvious OB associations. The UIT-selected sample is clearly more efficient in identifying candidate O-type stars than is using the APM data as an input catalogue. However, the UV-selected sample does not appear to reveal a new and distinct O-star population; a significant majority of the UIT targets observed with 2dF are early-B-type stars.

7.7 Individual objects

7.7.1 2dFS#0936

The spectrum of star #0936 has narrow, strong He II λ4686 emission with an equivalent width of -3.5Å ($\pm$ 0.2), and weaker N III and C III lines (see Fig. 17). The spectrum is classified here as O6.5 f?p, a category first introduced by Walborn (1972). The principal defining characteristic of Of?p stars is C III λ4647-50-51 emission comparable in intensity to N III λ4634-40-42, although the relative intensities of N III, C III and He II emission vary significantly in several well observed examples (Nazé et al. 2001; Walborn et al. 2003). Aside from the weaker C III emission, the spectrum of #0936 is similar to that of AzV 220 (Walborn et al. 2000); in common with AzV 220, #0936 is too faint (with $M(B) \simeq -5.0$) for a 'normal' supergiant, when compared to the calibration given by Walborn (1973). The spectrum also displays Balmer emission (unresolved at Hγ), the origins of which are not clear; the star is in H35 (Hodge 1985), which Bica & Schmitt (1995) list as type "AN – an association which shows some traces of H II emission."

Further observations of this star would be useful to distinguish between intrinsic and nebular emission, and to monitor for spectral variations. In the course of their survey for WR stars, Massey & Duffy (2001) observed 2dFS#0936 (their "Anon-1"), assigning a spectral type of O5 f?p. The 2dF spectrum (which has greater wavelength coverage) is not consistent with this classification, since He I λ4026 is stronger than He II λ4200. At the current time it is unclear whether this difference is attributable to differences in data quality or to intrinsic spectral variability.

7.7.2 2dFS#0999: SMC-WR 9

Star 2dFS#0999 (Fig. 17) was the ninth Wolf-Rayet (WR) star discovered in the SMC (Morgan, Vassiliadis & Dopita 1991). The strong N V emission, in combination with an absence of N IV, gives the WN2.5 type (van der Hucht 1996), and the absorption component is consistent with an O3 companion, based on the absence of He I λ4471. The spectrum has previously been classified as WN2.5+O5: (Morgan et al. 1991) and WN3+O3–4 (Massey & Duffy 2001). The 2dF spectrum has resolution comparable to Morgan's data, and a comparison shows the N V to He II λ4686 ratio has apparently increased.

7.7.3 2dFS#3235: AzV 490/Sk 160

The 2dF spectrum of 2dFS#3235 (AzV 490; Sk 160 in the catalogue of Sanduleak 1968) shows strong He II emission at λ4686. This is the optical counterpart of SMC X-1. The optical spectrum has long been known to be variable (e.g., Osmer & Hiltner 1974), and our RGO spectrum shows differences from the 2dF spectrum (e.g., He II λ4686

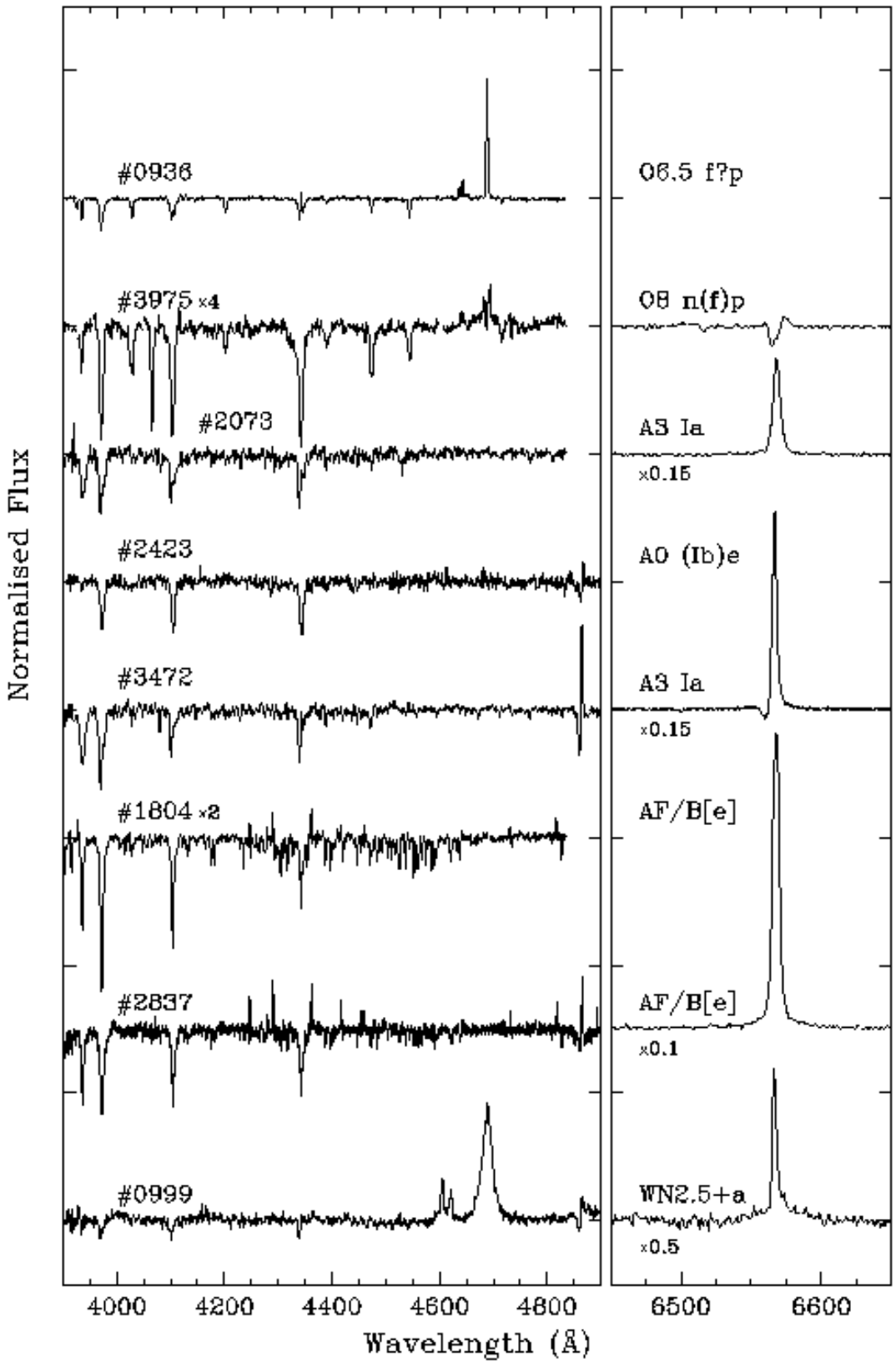

Figure 17. Objects of particular interest, identified by 2dFS number; see Sections 7.3 and 7.7 for a discussion of the spectra shown. Tickmarks on the y axis are every 1.0 continuum units.

double-peaked in the former, single-peaked in the latter). Our 2dF spectrum is very similar to that of HDE 269896 in the LMC, classified as ON9.7 Ia+ (Walborn 1977, Walborn & Fitzpatrick 1990).

7.7.4 2dFS#3472; #2073, #2423

2dFS#3472 (A3 Ia) is an emission-line object, previously catalogued as Lin 530 and MA93-1879 (Lindsay 1961; Meyssonnier & Azzopardi 1993). RGO (Hα) and 2dF (blue-region) spectra are shown in Fig. 17. Although Balmer-line emission is not particularly rare in luminous Galactic A supergiants, the P-Cygni Hα line in 2dFS#3472 is exceptionally strong, with an emission equivalent width of $\sim$40Å.

2dFS#2423 (A0 (Ib)) is the only other A-type star in our catalogue showing clear P-Cygni emission at Hβ, albeit rather weaker than in #3472, while 2dFS#2073 (A3 Ia) shows probable P-Cygni emission at Hγ, together with strong Hα P-Cygni emission (Fig. 17).

7.7.5 2dFS#3975: Sk 190

The spectrum of star #3975 (Fig. 17) is classified here as O8n(f)p. The primary requirement for membership of this class is a composite emission and absorption structure in the He II λ4686 line (Walborn 1973). The 2dF spectrum was both noisy and near the edge of the engineering-grade chip in the 1998 observations, introducing assorted cosmetic features; subsequent observation with the RGO spectrograph confirmed the classification. This is only the second Onfp spectrum seen in the SMC, after AzV 80 (Walborn et al. 2000). Sk 190 has previously been classified as O8 Iaf (Massey 2002), suggesting the possibility of time variability in the intensity and morphology of the He II λ4686 line.

8 ACKNOWLEDGEMENTS

CJE was funded by PPARC during the course of this work. This paper is based on data obtained with the Anglo-Australian Telescope, and we thank the staff of the observatory (particularly Russell Cannon) for their support. Ed Fitzpatrick, Richard Gray, and our referee, Nolan Walborn, provided helpful comments, and we also thank Martin Cohen, Danny Lennon, and Nidia Morrell for useful correspondence.

REFERENCES

Abt H. A., 1981, ApJS, 45, 437
Abt H. A., 1985, ApJS, 59, 95
Ardeberg A., 1980, A&AS, 42, 1
Azzopardi M., 1982, in The Most Massive Stars p. 227
Azzopardi M., 1987, A&AS, 69, 421
Azzopardi M., Vigneau J., 1975, A&AS, 22, 285
Azzopardi M., Vigneau J., 1982, A&AS, 50, 291
Baade D., Rivinius T., Štefl S., Kaufer A., 2002, A&A, 383, L31
Balona L., Crampton D., 1974, MNRAS, 166, 203
Bica E., Dutra C. M., 2000, AJ, 119, 1214
Bica E. L. D., Schmitt H. R., 1995, ApJS, 101, 41
Blair M., Gilmore G., 1982, PASP, 94, 742
Chromey F. R., Hasselbacher D. A., 1996, PASP, 108, 944
Cornett R. H., Greason M. R., Hill J. K., Parker J. W., Waller W. H., 1997, AJ, 113, 1011
Cowley A., Cowley C., Jaschek M., Jaschek C., 1969, AJ, 74, 375
Evans C. J., Howarth I. D., 2003, MNRAS, 345, 1223
Fehrenbach C., Duflot M., 1972, A&A, 21, 321
Fitzgerald M. P., 1970, A&A, p. 234
Garmany C. D., Conti P. S., Massey P., 1987, AJ, 93, 1070
Gilmore G., Howell D., eds, 1998, The Stellar Initial Mass Function, 38th Herstmonceux Conference. A.S.P. Conference Series, Vol. 142
Gray R. O., Garrison R. F., 1987, ApJS, 65, 581
Gray R. O., Garrison R. F., 1989, ApJS, 70, 623
Gray R. O., Napier M. G., Winkler L. I., 2001, AJ, 121, 2148
Harries T. J., Hilditch R. W., Howarth I. D., 2003, MNRAS, 339, 157
Henize K. G., 1956, ApJS, 2, 315
Heydari-Malayeri M., 1990, A&A, 234, 233
Hodge P. W., 1985, PASP, 97, 530
Hummel W., Szeifert T., Gässler W., Muschielok B., Seifert W., Appenzeller I., Rupprecht G., 1999, A&A, 352, L31
Humphreys R. M., 1983, ApJ, 265, 176
Humphreys R. M., Kudritzki R. P., Groth H. G., 1991, A&A, 245, 593
Humphreys R. M., McElroy D. B., 1984, ApJ, 284, 565
Hutchings J. B., 1966, MNRAS, 132, 433
Jaschek C., Jaschek M., 1990, The Classification of Stars. Cambridge University Press
Keller S. C., Wood P. R., Bessell M. S., 1999, A&AS, 134, 489
Landolt A. U., 1992, AJ, 104, 372
Lennon D. J., 1997, A&A, 317, 871
Lewis I. J., Cannon R. D., Taylor K., Glazebrook K., Waller L. G., Whittard J. D., Wilcox J. K., Willis K. C., 2002, MNRAS, 333, 279
Lindsay E. M., 1961, AJ, 66, 169
Massey P., 2002, ApJS, 141, 81
Massey P., Duffy A. S., 2001, ApJ, 550, 713
Massey P., Lang C. C., DeGioia-Eastwood K., Garmany C., 1995, ApJ, 438, 188
Meyssonnier N., Azzopardi M., 1993, A&AS, 102, 451
Morgan D. H., Keenan P. C., 1973, ARA&A, 11, 29
Morgan D. H., Vassiliadis E., Dopita M. A., 1991, MNRAS, 251, 51
Morgan W. W., Code A. D., Whitford A. E., 1955, ApJS, 2, 41
Morgan W. W., Harris D. L., Johnson H. L., 1953, ApJ, 118, 92
Morgan W. W., Keenan P. C., Kellman E., 1943, An atlas of stellar spectra. Chicago Univ. Press
Morgan W. W., Roman N. G., 1950, ApJ, 112, 362
Nazé Y., Vreux J.-M., Rauw G., 2001, A&A, 372, 195
Osmer P., Hiltner W. A., 1974, ApJ, 188, L5
Parker J. W., 2002, in Crowther P. A., ed., The Earliest Stages of Massive Star Birth. A.S.P. Conference Series, Vol. 267, p. 401
Parker J. W., Hill J. K., Cornett R. H., Hollis J., Zamkoff E., Bohlin R. C., O'Connell R. W., Neff S. G., Roberts M. S., Smith A. M., Stecher T. P., 1998, AJ, 116, 180

Pietrzynski G., Udalski A., Kubiak M., Szymanski M., Wozniak P., Zebrun K., 1998, Acta Astronomica, 48, 175
Salpeter E. E., 1955, ApJ, 121, 161
Sanduleak N., 1968, ApJ, 73, 246
Sanduleak N., 1972, A&A, 17, 326
Schmidt-Kaler T., 1982, in Schaifers K., Voigt H. H., eds, Landolt-Börnstein, Group VI, Vol 2b Springer-Verlag, p. 1
Slettebak A., 1954, 1954, 119, 146
Udalski A., Szymański M., Kubiak M., Pietrzyński G., Woźniak P., Żebruń K., 1998, Acta Astron., 48, 147
van der Hucht K. A., 1996, in Vreux J. M., ed., Wolf-Rayet Stars in the Framework of Stellar Evolution; 33rd Liège Int. Astroph. Coll. p. 1
Walborn N. R., 1972, AJ, 77, 312
Walborn N. R., 1973, AJ, 78, 1067
Walborn N. R., 1977, ApJ, 215, 53
Walborn N. R., Fitzpatrick E. L., 1990, PASP, 102, 379
Walborn N. R., Howarth I. D., Herrero A., Lennon D. J., 2003, ApJ, 588, 1025
Walborn N. R., Lennon D. J., Heap S., Lindler D. J., Smith L. J., Evans C. J., Parker J. W., 2000, PASP, 112, 1243
Wegner W., 2000, MNRAS, 319, 771
Zaritsky D., Harris J., Thompson I. B., Grebel E. K., Massey P., 2002, AJ, 123, 855

APPENDIX A: CATALOGUE DESCRIPTION

The full catalogue of spectral types for the 2dF sample is available electronically through the on-line edition of Monthly Notices, and at the Centre de Données astronomiques de Strasbourg (CDS[6]). The data are assembled in two tables, one containing the basic observational data from the spectroscopic survey, and one containing cross-identifications.

Table A1 shows an extract from the data catalogue, to illustrate the format. For convenience, we assign a 4-digit 2dFS number to each star; entries 1–4054 are the main, APM-selected, targets, sorted by RA, and entries 5001–5107 are the UIT-selected targets, separately sorted by RA. There are no catalogue entries 4055–5000. For each entry we give the adopted co-ordinates and B magnitude (Section 5.4.2). Co-ordinates are quoted from the sources used for spectrograph fibre configuration, i.e., APM for 2dFS entries 1–4054, OGLE for entries 5001–5107 (cf. Harries et al. 2003). We then list the adopted 2dF spectral type, and notes on Balmer-line emission for Hα, Hβ, and Hγ, as available (Section 7.1). The overall distribution of spectral types is summarized in Table 7. Note that the luminosity classes for the A0 and B-type stars are given in parentheses, to reflect the fact that they are not based solely on morphological considerations and therefore are not strict 'MK' types.

The supplementary catalogue of cross-identifications includes full photometric results from Massey, OGLE, and MCPS (Section 5), and cross-identifications with the UIT, Sanduleak, AzV, and MA93 catalogues (Cornett et al. 1997; Sanduleak 1968, 1972; Azzopardi & Vigneau 1982; Meyssonnier & Azzopardi 1993). The catalogue also includes pertinent information from the catalogue of SMC clusters by Bica & Dutra (2000), which is, essentially, the catalogue of Bica & Schmitt (1995), with the inclusion of new clusters identified in the OGLE survey (Pietrzynski et al. 1998). Our purpose in including this information is to provide an indication of whether a given star is likely to be a cluster or association member, or a field star (relevant to the interpretation of the HRD).

There are 49 Sk stars matched in the 2dFS catalogue, 172 AzV stars, 219 MA93 stars, and 454 UIT stars (including 107 UIT-selected targets). These correspondences are to be understood to be simply positional matches for the photometric, UIT, and MA93 catalogues (which list co-ordinates to the nearest arcsecond or better), but are actual cross-identifications for the Sk and AzV catalogues, using published finder charts.

[6] `ftp://cdsarc.u-strasbg.fr/pub/cats/J/MNRAS/XXX/YYY`

Table A1. An illustrative section of the on-line 2dF catalogue. Sources of adopted B magnitudes are APM, Massey, OGLE, and Zaritsky (coded A, M, O, Z; see Section 5.4.2). The 'Balmer notes' summarize lines in blue (B: g=Hγ, b=Hβ) and red (R: Hα) spectra, coded as a (absorption); n (narrow [nebular?] emission); r (resolved [but narrow] emission); d (double-peaked emission); p (P-Cyg profile).

2dFS#	α (J2000)			δ (J2000)			B	Source	Spectral type	Balmer notes	
0600	00	46	23.13	−72	50	17.4	16.36	O	A3 II	B[ga]	R[n]
0601	00	46	28.15	−72	52	23.3	16.63	O	B8 (III)	B[ga bn]	
0602	00	46	28.40	−73	27	43.0	15.15	Z	B1–5 (II)	B[gn]	R[n]
0603	00	46	30.53	−72	26	58.4	16.84	Z	B1–5 (IV)	B[ga]	
0604	00	46	32.90	−72	25	16.8	16.53	Z	B0.5 (V)	B[ga]	
0605	00	46	33.08	−72	10	39.3	16.86	Z	B0–5 (V)	B[ga]	
0606	00	46	33.47	−73	39	25.8	13.34	M	B8 (Ib)	B[ga ba]	
0607	00	46	33.86	−73	53	04.7	17.60	Z	B0–5 (V)	B[ga ba]	
0608	00	46	35.12	−72	56	04.2	15.93	O	B3 (III)	B[ga ba]	
0609	00	46	38.10	−73	55	13.7	14.31	Z	B0.5 (IV)	B[ga]	
0610	00	46	40.19	−73	31	16.9	14.17	Z	O7–8 V	B[gn bn]	
0611	00	46	41.70	−74	00	49.0	17.11	Z	B0–5 (V)	B[gn bn]	
0612	00	46	43.21	−73	28	03.4	16.46	O	B1–5 (III)	B[ga bn]	R[n]
0613	00	46	46.20	−73	41	13.2	16.35	Z	B1–5 (III)	B[ga]	
0614	00	46	47.00	−73	58	29.7	17.42	Z	A3 II	B[ga ba]	
0615	00	46	47.38	−72	33	46.7	17.37	Z	F8	B[g]	
0616	00	46	47.72	−72	58	43.8	17.10	Z	B0–5 (V)	B[ga]	R[n]
0617	00	46	48.07	−73	57	10.6	16.88	Z	A2 III	B[ga ba]	
0618	00	46	48.95	−73	30	37.3	16.66	O	B8–A0 (II)	B[gn bn]	
0619	00	46	50.81	−72	17	10.9	15.78	Z	B0–5 (II)	B[gr]	
0620	00	46	50.88	−73	55	21.5	14.57	Z	B2 (III)	B[ga]	